

# Numerical Heat Transfer, Part A: Applications

## An International Journal of Computation and Methodology

ISSN: (Print) (Online) Journal homepage: <https://www.tandfonline.com/loi/unht20>

---

# Heat and mass transfer phenomenon and aligned entropy generation with simultaneous effect for magnetized ternary nanoparticles induced by ferro and nano-layer fluid flow of porous disk subject to motile microorganisms

Qadeer Raza, Xiaodong Wang, Bagh Ali, M. Zubair Akbar Qureshi & Ali J. Chamkha

To cite this article: Qadeer Raza, Xiaodong Wang, Bagh Ali, M. Zubair Akbar Qureshi & Ali J. Chamkha (22 Dec 2023): Heat and mass transfer phenomenon and aligned entropy generation with simultaneous effect for magnetized ternary nanoparticles induced by ferro and nano-layer fluid flow of porous disk subject to motile microorganisms, Numerical Heat Transfer, Part A: Applications, DOI: [10.1080/10407782.2023.2292767](https://doi.org/10.1080/10407782.2023.2292767)

To link to this article: <https://doi.org/10.1080/10407782.2023.2292767>



Published online: 22 Dec 2023.



Submit your article to this journal [↗](#)



View related articles [↗](#)





View Crossmark data [↗](#)

---



# Heat and mass transfer phenomenon and aligned entropy generation with simultaneous effect for magnetized ternary nanoparticles induced by ferro and nano-layer fluid flow of porous disk subject to motile microorganisms

Qadeer Raza<sup>a</sup> , Xiaodong Wang<sup>a</sup>, Bagh Ali<sup>b</sup>, M. Zubair Akbar Qureshi<sup>c</sup>, and Ali J. Chamkha<sup>d</sup> 

<sup>a</sup>School of Mathematics and Statistics, Xian Key Laboratory of Scientific Computation and Applied Statistics, Northwestern Polytechnical University, Xian, China; <sup>b</sup>School of Mechanical Engineering and Automation, Harbin Institute of Technology, Shenzhen, China; <sup>c</sup>Department of Mathematics, Air University, Islamabad, Multan, Pakistan; <sup>d</sup>Faculty of Engineering, Kuwait College of Science and Technology, Doha District, Kuwait

## ABSTRACT

This articles focus the dynamics of fluid conveying ternary solid particles, nano-layer, and magnetic field effects subject to porous disks. The magnetized ternary nanoparticles induced by Ferro and nano-layer are considered due to their unusual characteristics like extraordinary thermal conductivity, which are significant in advanced nanotechnology, heat exchangers, material sciences, and electronics. To avoid possible sedimentation of tiny particles, the motile microorganisms are also considered in the elaborated fluid problem. The main objective of this comprehensive study is the enhancement of heat transportation. In this study, we also investigate the physical dynamics of entropy generation, particularly emphasizing viscous dissipation related to joule heating effects. The mass transfer equation was employed to monitor the chemical interaction with diverse nanoparticles. The results of comparative and numerical validation agree well. The approach of stable and accurate numerical boundary value problem of fourth order code (bvp4c) is applied to solve the nonlinear system of ordinary differential equations. Many useful engineering results are summarized here, including the skin friction coefficient ( $C_f$ ), Nusselt number (Nu), Sherwood number (Sh), and motile number (Nn). For both porous disks, several non-dimensional parameter effects are depicted graphically and tabulated. The results show that the increasing the number of nano-layer particles slows the rate of the temperature profile in both porous disks, associated with the expansion ratio, Reynolds number, and magnetic field number. Moreover, increasing the values of the density ratio number results in an increase in the flow of microorganisms profile in both porous disks. Increasing the values of the diffusivity parameters and the temperature difference enhances the flow of entropy generation.

## ARTICLE HISTORY




Received 30 September 2023  
Revised 28 November 2023  
Accepted 30 November 2023

## KEYWORDS

Entropy generation; heat and mass transfer in the flow of motile microorganisms; ternary hybrid ferrofluids; thermal conductivity of nanolayer; viscous dissipation and joule heating effect

## 1. Introduction

Entropy generation ( $E - G$ ) refers to the amount of irreversible dissipation of energy that occurs during a thermodynamic process. It is a measure of the inefficiency of a system in converting energy into work. In practical applications, entropy generation plays a key role in determining

**CONTACT** Xiaodong Wang  xiaodongwang@nwpu.edu.cn; Qadeer Raza  qadeerraza@mail.nwpu.edu.cn  School of Mathematics and Statistics, Xian Key Laboratory of Scientific Computation and Applied Statistics, Northwestern Polytechnical University, Xian 710129, China.

### Nomenclature

$B_0$	Uniform magnetic field	$Sh$	Sherwood number
$F_\eta$	Dimensionless radial velocity profile	$Nn$	Motile number
$G_\eta$	Dimensionless tangential velocity profile	$(u, v, w)$	Velocity component along z axis
$\theta(\eta)$	Temperature profile	$(r, 0, z)$	Cylindrical coordinates system
$\chi(\eta)$	Concentration profile	$\eta$	Independent similarity variable
$\psi(\eta)$	Microorganism profile	$\phi$	Equivalent nanoparticles volume fraction
$N_s$	Entropy generation	$\sigma$	Electrical conductivity
$N$	Density of motile number	$A_1$	Dimensional less parameter
$Pe$	Peclet number	$s(t)$	Time depended on coefficient
$C_f$	Skin friction coefficient	$\mu$	Dynamic viscosity
$Nu$	Nusselt number		

the efficiency of various processes such as power generation, refrigeration, and combustion. It is critical to reduce entropy output in order to improve the efficiency of these processes and reduce waste.  $E - G$  is closely related to the second law of thermodynamics, which states that the total entropy of a closed system always increases over time. Therefore, understanding and controlling  $E - G$  is crucial for designing and optimizing energy-efficient systems. Overall, entropy generation provides a valuable tool for analyzing the thermodynamic efficiency of various processes and designing more sustainable technologies. Recent studies have looked into  $E - G$  with a porous disk can improve thermal efficiency and system conductivity. Bhandari et al. [1] studied the movement and thermal transfer properties of a water-based CNTs ferrofluid between two radially extensible spinning disks in the influence of a uniform magnetic field, as well as  $E - G$ . Acharya et al. [2] determined the flow of hybrid nanofluid (HNFD) thermal and concentration profile under the effect of magneto-hydrodynamic (MHD) caused by a revolving disk, taking into account  $E - G$ , thermal radiation, convection situations, momentum, and concentrating slips. Ibrahim et al. [3] exploited thermal infrared reflection source/sink influence to evaluate the heat transport process in the flow of ternary hybrid nanofluid (THNFD), as well as the impacts of  $E - G$  on the flow. Thermal radiation and the impacts of heat sources and sinks are employed to investigate the thermal transfer mechanism. Also, the flow of ternary hybrid nanofluid's  $E - G$  has been examined by Ramzan et al. [4]. Agrawal et al. [5] research is to investigate the HNFD squeezing flow across two simultaneous disks. The second rule of thermodynamics is used to evaluate  $E - G$  investigation, and Darcy's mode entails predicting the performance of porous materials. In the existence of Hall current, heat flux, and viscoelastic dispersion, Divya et al. [6] examined  $E - G$  in MHD (HNFD) flow over an unstable spinning disk. On a permeable spinning disk under the impact of thermal radiation, heat generation, and viscous dissipation, Ramasekhar et al. [7] investigated the  $E - G$  of a HNFD. Shah et al. [8] investigated the Prandtl-Eyring nanofluid with base fluid engine oil flowing across a heat extending interface with entropy production and parameter transfer examination in the current study. Farooq et al. [9] explore the effects of suction/injection and viscous dissipation on  $E - G$  in the boundary layer flow of an (HNFD) over a nonlinear radially stretching porous disk. Mahesh et al. [10] focused on optimizing  $E - G$  in radiative MHD fluid flow combined with (HNFD) and mono (NFD), revolving around two chemical reaction disks.

Nanofluid (NFD) is a fluid that contains tiny-particles of having diameter at-least 100 nanometers, they are mixed into the base fluid to improve its thermal and transport characteristics. In order to generate a more effective heat transfer fluid, two distinct types of nanoparticles are combined and distributed in a base fluid to form a HNFD. A base fluid is mixed with three distinct kinds of nanoparticles to create a ternary hybrid nanofluid (THNFD). When these fluids are used in the flow through porous disks, they can significantly improve the heat transfer rate due to

their enhanced thermal properties. This makes them useful in a range of applications, including the cooling of electronic devices, solar collectors, and automotive cooling systems. Overall, the use of NFDs, HNFDs, and THNFDs in porous disk flow offers a promising way to enhance heat transfer efficiency and reduce energy consumption in various engineering systems. Numerous researchers have conducted work on THNFDs. In their recent study, Arif et al. [11] researched the suspension of three distinct types of nanoparticles in a variety of forms for advanced cooling applications in engineering challenges and industries. This study considers a revolving disk with viscoelastic radiative THNFDs. Shahzad et al. [12] was to determine the thermal properties of THNFDs by examining the ternary nanoparticles (NPs) that affected the fluid flow and heat transfer across spinning disks. Utilizing kinetic energy, Hall current, and heat degeneracy calculations, Shamsuddin et al. [13] examined the combining of THNFDs in MHD flow or overflow of a rotating disk. Zeeshan et al. [14] studied two-way flow with water and hydrogen bubbles in a flexible channel, using the Rayleigh-Plesset equation to accurately model hydrogen void formation. A deep study of thermal radiations upon a constant 2 dimensional movement of THNFDs across a spinning disk with slip border settings as well as a constant magnetic field, as per the analysis of Alshahrani et al. [15]. exposed the impact a spinning disk with the an immiscible force with the significance hall current. Three different types of metallic oxide nanoparticles make up the THNFDs flow. Usman et al. [16] examine the effect of a time-varying magnetic field on the unsteady slip flow of a THNFDs across an inclined spinning disk, as well as the related heat transfer process. According to Alanazi et al. [17] investigation completely developed HNFDs are used to achieve the 3D flow over rotating permeable disks as well as a ringed sector. An infinitely long impermeable spinning disk is the subject of research by Tassaddiq et al. [18]. Zhang et al. [19] examined the 3D numerical approach of an unsteady Ag-MgO/water HNFDs flow involving energy as well as thermal transmission created by an oscillating disk with upward and downward motion. Waini et al. [20] work aims to investigate the erratic flow over a rotating disk for HNFDs with suction as well as retaliating characteristics. Agrawal et al. [21] assessed the effectiveness of heat conduction as well as the flow characteristics of HNFDs across two parallel disks. Zeeshan et al. [22] examined the impact of fluid particles on curved structure twisting, considering mass and heat transfer, and applied that to biological fluid movement in small muscles. Alharbi et al. [23] study on the magnetized Jeffrey fluid's peristaltic flow in a rotating planar channel provided valuable insights into the complex dynamics of this system that have significant applications in engineering and biomedical fields. Majeed et al. [24] conducted numerical investigations on intricate double stratification impact with a radiative mixed convective nanofluid over a cylinder.

An important factor variable viscosity is considered in various heat transfer applications, including electronics cooling, chemical reactions, and solar thermal systems. Viscous dissipation can cause the conversion of kinetic energy to internal energy due to shear stresses, leading to an increase in temperature. Joule heating occurs due to electrical resistance in a fluid, leading to the generation of heat. Enhancing the capacity and effectiveness of thermal transfer techniques requires tight control over these effects. In electronics cooling, these effects can reduce the efficiency of the system, leading to higher temperatures and potential failure. In contrast, in certain chemical reactions and solar thermal systems, these effects can enhance heat transfer and improve the overall efficiency of the system. Overall, understanding and controlling the impact of temperature dependent viscosity is essential for developing efficient and effective heat transfer systems in a range of applications. For the case of strong, uniform suction, in a disk traveling at such a high speed in an electric field. Regarding the intensity of the magnetic flux as well as the disk rotational speed, the rate of heat flux is measured with a VDAJH. The merged consequences of VDAJH on steady MHDs, the existence of Hall and the fluid stream over a slip regarding the electrical conductivity across a disk, are analyzed by Osalusi et al. [25]. Iqbal et al. [26] studied the mass transmission as well as heat transmission through an unsteady hydromagnetic highly

conductive immiscible water-based viscous HNFs (including titanium dioxide Nan particles) among two perpendicularly rotating porous coaxial disks exhibiting suction and VDAJH. Energy transfer under VDAJH is studied. According to Alanazi et al. [17], completely developed HNFs with VDAJH analysis are used to carry out 3D flow *via* rotating permeable disks. Zeeshan et al. [27] studied the impact of  $\text{Al}_2\text{O}_3$  nanoparticle shapes and sinusoidal waves on the flexible outer cylinder wall on the flow of an aqueous medium in the porous space between eccentric cylinders, with the inner cylinder rotating at a constant speed. Ijaz et al. [28] studied drug particle behavior in a non-Newtonian fluid, controlling transport using magnetic force lines perpendicular to the flow direction.

An investigation in the sub-field physics on the dynamics of electrically conductive fluids in the presence of magnetic fields known as Magnetohydrodynamics (MHD). In MHD, magnetic fields can influence the motion of the fluid and vice versa, leading to various phenomena such as electromagnetic induction, Faraday's law, and Lorentz forces. There are several uses for MHD, including in plasma physics, astrophysics, and engineering, such as in the design of fusion reactors, magnetic flow meters, and electromagnetic pumps. MHD can also be used in the development of novel energy conversion systems, such as MHD generators, which can convert the kinetic energy of high-temperature gases into electrical energy without the need for moving parts. Overall, MHD provides a valuable tool for understanding and manipulating the behavior of electrically conducting fluids in a range of applications. Numerous researchers have examined the application of HNFs in MHD, which has become a well-researched and well-known field. Heat transmission of HNFs through a circular disk with MHD action was explored by Shoaib et al. [29]. Using a radially pushed disk, Chaudhary et al. [30] presented study on 2D radially symmetric MHD stationary circulation of  $(\text{TiO}_2\text{-CuO/EG})$  HNFs. Neha et al. [31] investigated the Magneto hydrodynamic (MHD) HNFs flow disrupted with a slowdown spinning disk consisting of Ohmic heating, Sorbet, as well as DuFour upshot. In a study by Reddy et al. [32], Silver water, as well as copper-water HNFs (volume portions of 1 and 4%), were tested for their features of thermal and mass transmission up a spinning disk across a permeable media. Ouyang et al. [33] study the fluid stream with hybrid particles in three dimension past a spinning plate with the impact of magnetic field acting onward the cross direction to the stream. HNF flow across a rotating plate was investigated by Tassaddiq et al. [18]. To more thoroughly explore the precise mark of HNF flow, the influence of a magnetic region has been accumulated.  $\text{Al}_2\text{O}_3 - \text{Cu}/\text{H}_2\text{O}$  HNFs flow through a satellite force disk was examined by Yahaya et al. [34] using a convection frontier setting, viscous-Ohmic mixing, in addition, a magnetic field is imposed. Majeed et al. [35] studied the MHD flow of silver/water nanofluid past a stretched cylinder under the influence of thermal radiation with chemical reaction and slip conditions.

Nanolayer thermal conductivity refers to the ability of a thin layer of material with nanoscale thickness to conduct heat. In nanolayer thermal conductivity, the thermal conductivity of the material can be significantly different than that of the bulk material, due to the increased surface area and changes in the crystal structure at the nanoscale. Nanolayer thermal conductivity has important implications for various applications, including thermal management in electronics, thermoelectric devices, and energy conversion systems. By manipulating the properties of the nanolayers, it is possible to enhance the thermal conductivity of the material, leading to improved heat transfer efficiency and overall system performance. The study of nanolayer thermal conductivity is an active area of research, with ongoing efforts to better understand the fundamental mechanisms and develop new materials with improved thermal properties. Overall, nanolayer thermal conductivity provides a promising approach for developing advanced materials and technologies for efficient heat transfer in various applications. The current study reveals in detail how nanolayers affect nanofluidic transit as well as, Qureshi et al. [36] studied heat transfer properties and fluid flow dynamics in MHD hybrid nanofluids over a disk, enhancing understanding and potential applications in advanced materials engineering, energy efficiency, and thermal

management solutions. Raza et al. [37] studied heat and mass transfer processes in nanolayers, influenced by morphology, microorganisms, and magneto hydrodynamics over a disk. They examined viscous dissipation from Joule heating effects in ternary hybrid nanofluids, optimized impact on convective heat transfer coefficient, and optimization for microelectronic cooling and solar thermal systems. Acharya et al. [38] studied unsteady ferrous-water nano-liquid flow over a spinning disk, examining the influence of solid-liquid inter facial layer and nanoparticle diameter, velocity slip, and low-oscillating magnetic field, revealing hydrothermal implications. Fatima et al. [39] developed a mathematical model to represent magneto hydrodynamic effects on a two-phase pumping flow, revealing the importance of rotational blood flows in medical science and their connection to healthy cardiac function. Ijaz et al. [40] evaluated the effects of electro-kinetic force on the channel walls caused by the presence of an electrical charge layer, and the nano-bio-fluid filling the space between two concentric curved plates. Zeshan et al. [22] studied bio-inspired pumping systems, which use mechanisms like peristalsis and complex fluids to enhance efficiency. They also explored the use of flexible materials mimicking natural organism movements for improved propulsion capabilities. Majeed et al. [41] investigated the influence of magnetized Casson nanofluid flow and heat transport phenomena on a boundary layer flow over a nonlinear stretchable surface in their paper.

Heat and mass transfer (HAMT) in the flow of motile microorganisms is a complex process that is influenced by various factors, including the properties of the microorganisms, their swimming behavior, and the surrounding fluid. The motility of microorganisms can enhance heat and mass transfer by creating mixing and flow structures, while their consumption and transport of mass can alter the concentration gradients and flow patterns. The study of heat and mass transfer in the flow of motile microorganisms has important implications for various applications, including bioprocessing, food and beverage industries, and environmental engineering. In bioprocessing, understanding the behavior of motile microorganisms can aid in the optimization of microbial production processes. In the food and beverage industry, microorganisms can be used for fermentation processes, where heat and mass transfer are key factors for product quality and yield. In environmental engineering, motile microorganisms can be utilized in wastewater treatment processes, where they help to remove pollutants and enhance mass transfer rates. Overall, understanding the interplay between motile microorganisms and heat and mass transfer is essential for designing and optimizing processes in various industries. Bilal et al. [42] investigated the numerical modeling fluid flow with hybrid particles along moving microorganisms with the significance of CNTs. The frontier layer stream with microscopic organisms over the spongy disk are the major topics of the mathematical design presented by Naveed et al. [43]. Khan et al. [44] study the shifting disk along no mass flow created by HNFs with moving microorganisms. Impact of microorganisms along NPs getting by two extended or narrow disks investigated, Hussain et al. [45] presented the underlying properties of magnetic crossed convective flow. A mathematical study of von-Karman whirling flow over extended disk with porous media drenched and loaded with the movement of microorganisms was described by Beg et al. [46] in their work. Fatima et al. [47] analyzed a model for the peristaltic flow of nanofluid in a conductive channel and used Debye-Hückel and lubrication theory approximations to solve the electric potential function. Ijaz et al. [48] studied heat transfer's impact on solid particle motion in MHD Ree-Eyring fluid, examining its velocity, temperature profiles, particle motion, and dispersion characteristics. Raza et al. [49] study explores heat and mass transfer in porous disk systems using hybrid nanofluids made of (Ag – Al<sub>2</sub>O<sub>3</sub>) nanoparticles suspended in water, further enhances understanding of convective heat and mass transfer processes, reveals the influence of advanced nanolayer thickness formulations. Li et al. [50] conducted an analysis indicating that bioconvection in fluids can be significantly influenced by melting thermal transport, particularly in the context of heat transfer and energy transmission. In the work by Majeed et al. [51], the examination focuses on the flow of bio-convective nanoparticles in fluid and the electrically conducting, incompressible magneto-hydrodynamic flow

of nanofluid toward a chemically reactive stretchable surface. Fatima et al. [52] proposed a thermo-electric system dependent on the heat flow of nanomaterials, fractional volume of nanomaterial, density, and motile microorganisms. Jafar et al. [53] explored the 2D steady boundary layer mixed convection flow and heat transfer in ferromagnetic fluid over a stretching sheet. In another study, Majeed et al. [41] delved into the 2D bioconvection magneto-hydrodynamic (MHD) flow and heat transfer of the non-Newtonian (Casson) nanofluid model. Zeeshan et al. [54] aimed to explore the boundary layer heat transport flow of multiphase magnetic fluid with solid impurities suspended homogeneously past a stretching sheet under the impact of a circular magnetic field.

The authors conducted a comprehensive literature review and found that no previous research has explored the entropy generation resulting from the impact of morphological nanolayers on ternary hybrid MHD ferrofluid with the dispersion of magnetized nanocomposite materials. The study investigates the impact of morphological nanolayers on the thermal conductivity of ternary hybrid ferrofluids (THFFDs) in a doubly permeable porous disk. It considers factors like viscous dissipation and joule heating. Using the similarity variable method, the results are transformed into dimensionless ordinary differential equations (ODEs). The Bvp4c solver is used to tackle the 4th and 2nd-order ODEs. The study compares thermal conductivity and nanolayer thermal conductivity for magnetized ferrofluid nanoparticles. It also examines the impact of non-directional parameters like shear stress, tangential stress, skin friction coefficient, Nusselt number, Sherwood number, Motile number, velocity, temperature, concentration, microorganisms, and entropy generation. The main objective is to assess the influence of nanolayer thickness, nanoparticle diameters, and diffusivity parameters on entropy generation.

## 2. Mathematical formulation

Heat and mass transfer flow of motile microorganism with the entropy nanolayer generation of incompressible, time-dependent, 3D, chemical reaction, MHD, viscous dissipation and joule heating effects, across a magnetize nanoparticles moving two orthogonal permeable disks. When the tri hybrid magnetize nanoparticles ( $\text{Fe}_3\text{O}_4 + \text{CoFe}_2\text{O}_4 + \text{Mn} - \text{ZnFe}_2\text{O}_4/\text{H}_2\text{O}$ ) are combined, they form a complex mixture of magnetic nanoparticles that can have various applications in biomedicine, catalysis, and magnetic separation. In magnetic separation, the mixture of magnetic NPs can be used to separate different materials based on their magnetic properties. By applying an external magnetic field, the NPs can be used to selectively separate materials based on their magnetic susceptibility. Due to the extremely low Reynolds number values, the resultant magnetic force is ignored. When the applied magnitude of an outside magnetic force is along the z-axis. The diameter  $2r$  porous disk border is oscillating up and down. Motion along the cylindrical coordinates of fluid  $V = (u(r, z, \text{ and } t), v(r, z, \text{ and } t), \text{ and } w(r, z, \text{ and } t))$  is given in the physical model. Table 1 shows the base fluid and different magnetic NPs thermophysical properties. Where,  $T_1, T_2, C_1, C_2, N_1,$  and  $N_2,$  represents temperature, concentration, and motile microorganisms terms with the impact of lower and upper porous disk, and entropy generation illustrated in Figure 1. System of model equations is based on the above-mentioned supposition [55–60]:

Continuity equation

$$\frac{\partial u}{\partial r} + \frac{u}{r} + \frac{\partial w}{\partial z} = 0, \quad (1)$$

**Table 1.** Different magnetic NPs and base fluid thermo-physical properties.

	Base fluid (H <sub>2</sub> O)	Fe <sub>3</sub> O <sub>4</sub> ( $\phi_1$ )	CoFe <sub>2</sub> O <sub>4</sub> ( $\phi_2$ )	Mn – ZnFe <sub>2</sub> O <sub>4</sub> ( $\phi_3$ )
$C_p$ (J.(kg.K) <sup>-1</sup> )	997.0	5180	4907	4900
$\rho$ (kg.m <sup>-3</sup> )	4180	670	700.0	800
$\kappa$ (W.(m.K) <sup>-1</sup> )	0.6071	9.7	3.7	5

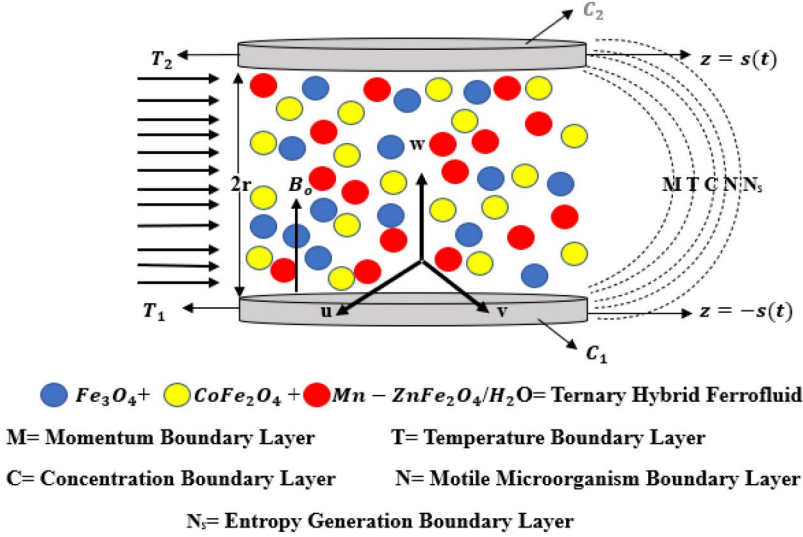


Figure 1. Physical model.

Three-dimensional momentum equation

$$\frac{\partial u}{\partial t} + u \frac{\partial u}{\partial r} + w \frac{\partial u}{\partial z} - \frac{v^2}{r} = -\frac{1}{\rho_{\text{trihffd}}} \frac{\partial p}{\partial r} + \left( \frac{\mu_{\text{trihffd}}}{\rho_{\text{trihff}}} \right) \left( \frac{\partial^2 u}{\partial r^2} + \frac{1}{r} \frac{\partial u}{\partial r} - \frac{u}{r^2} + \frac{\partial^2 u}{\partial z^2} \right) - \frac{\sigma_e B_0^2}{(\rho_{Cp})_{\text{trihffd}}} u, \quad (2)$$

$$\frac{\partial v}{\partial t} + u \frac{\partial v}{\partial r} + w \frac{\partial v}{\partial z} + \frac{uv}{r} = \left( \frac{\mu_{\text{trihffd}}}{\rho_{\text{trihff}}} \right) \left( \frac{\partial^2 v}{\partial r^2} + \frac{1}{r} \frac{\partial v}{\partial r} - \frac{v}{r^2} + \frac{\partial^2 v}{\partial z^2} \right) - \frac{\sigma_e B_0^2}{(\rho_{Cp})_{\text{trihffd}}} v, \quad (3)$$

$$\frac{\partial w}{\partial t} + u \frac{\partial w}{\partial r} + w \frac{\partial w}{\partial z} = -\frac{1}{\rho_{\text{trihffd}}} \frac{\partial p}{\partial z} + \left( \frac{\mu_{\text{trihffd}}}{\rho_{\text{trihff}}} \right) \left( \frac{\partial^2 w}{\partial r^2} + \frac{1}{r} \frac{\partial w}{\partial r} + \frac{\partial^2 w}{\partial z^2} \right) - \frac{\sigma_e B_0^2}{(\rho_{Cp})_{\text{trihffd}}} w, \quad (4)$$

Temperature equation

$$\frac{\partial T}{\partial t} + u \frac{\partial T}{\partial r} + w \frac{\partial T}{\partial z} = \alpha_{\text{trihffd}} \frac{\partial^2 T}{\partial z^2} + \frac{\mu_{\text{trihffd}}}{(\rho_{Cp})_{\text{trihffd}}} \left( \frac{\partial u}{\partial z} \right)^2 + \frac{\sigma_e B_0^2}{(\rho_{Cp})_{\text{trihffd}}} u^2, \quad (5)$$

Concentration equation

$$\frac{\partial C}{\partial t} + u \frac{\partial C}{\partial r} + w \frac{\partial C}{\partial z} = (D_b)_{\text{trihffd}} \left( \frac{\partial^2 C}{\partial z^2} \right) - K_o(C - C_2), \quad (6)$$

Motile microorganism equation

$$\frac{\partial N}{\partial t} + u \frac{\partial N}{\partial r} + w \frac{\partial N}{\partial z} + \frac{bW_c}{(C_1 - C_2)} \frac{\partial}{\partial z} \left( N \frac{\partial C}{\partial z} \right) = (D_n)_{\text{trihffd}} \left( \frac{\partial^2 N}{\partial z^2} \right), \quad (7)$$

Entropy generation equation

$$s'''_{\text{Gen}} = \frac{K_{\text{trihffd}}}{T_2^2} \left( \frac{\partial T}{\partial z} \right)^2 + \frac{\mu_{\text{trihffd}}}{T_2} \left( \frac{\partial u}{\partial z} \right)^2 + \frac{\sigma_e B_0^2}{T_2} u^2 + \frac{RD}{C} \left( \frac{\partial C}{\partial z} \right)^2 + \frac{RD}{N} \left( \frac{\partial N}{\partial z} \right)^2 + \frac{RD}{T_2} \left( \frac{\partial C}{\partial z} \frac{\partial T}{\partial z} \right) + \frac{RD}{T_2} \left( \frac{\partial N}{\partial z} \frac{\partial T}{\partial z} \right), \quad (8)$$

where  $\rho_{\text{trihffd}} = (\phi_1 \rho_{s1} + \phi_2 \rho_{s2} + \phi_3 \rho_{s3} + (1 - \phi_1 - \phi_2 - \phi_3) \rho_{\text{bf}})$  show the density of THFFDs,  $\phi_1, \phi_2, \phi_3, \rho_{s1}, \rho_{s2}, \rho_{s3}$ , and  $\rho_{\text{bf}}$  are represented by 1st, 2<sup>nd</sup>, or 3rd NPs volume fraction and density

of the solid and base fluid,  $\nu_{\text{trihffd}} = \frac{\mu_{\text{trihffd}}}{\rho_{\text{trihffd}}}$  stands for the kinematic viscosity of THFFDs,  $\mu_{\text{trihffd}} = \mu_{\text{bf}}(1 + 0.1008((\phi_1)^{0.69574}(dp_1)^{0.44708} + (\phi_2)^{0.69574}(dp_2)^{0.44708} + (\phi_3)^{0.69574}(dp_3)^{0.44708}))$  denoted by the dynamic viscosity of THFFDs,  $(dp)_1, (dp)_2,$  and  $(dp)_3$  are show the several types of NPs diameter,  $(\rho C_p)_{\text{trihffd}} = \phi_1(\rho C_p)_{s_1} + \phi_2(\rho C_p)_{s_2} + \phi_3(\rho C_p)_{s_3} + (1 - \phi_1 - \phi_2 - \phi_3)(\rho C_p)_{\text{bf}}$  demonstrated that the specific heat capacity of THFFDs,  $(\rho C_p)_{s_1}, (\rho C_p)_{s_2}, (\rho C_p)_{s_3}$  and  $(\rho C_p)_{\text{bf}}$  are illustrate the specific heat capacity of 1st, 2nd, or 3rd solid and liquid base fluid,  $\alpha_{\text{trihffd}} = \frac{k_{\text{trihffd}}}{(\rho C_p)_{\text{trihffd}}}$  illustrates the tri-hybrid nanolayer ferrofluid thermal diffusivity,  $\sigma_e$  show that the electrical conductivity,  $(W_c)$  represented by cell swimming velocity,  $(B_0)^2$  stand for the strong magnetic field, this term  $(\frac{\sigma_e B_0^2}{(\rho C_p)_{\text{trihffd}}})$  demonstrated by the MHD in Eqs. (2–4) right hand side, this term  $(\frac{\mu_{\text{trihffd}}}{(\rho C_p)_{\text{trihffd}}} (\frac{\partial u}{\partial z})^2 + \frac{\sigma_e B_0^2}{(\rho C_p)_{\text{trihffd}}} u^2)$  represented by the Viscous dissipation and Joule heating effects in Eq. (5),  $(K_0(C - C_2))$  show a chemical reaction term denoted in Eq. (6),  $(\frac{K_{\text{trihffd}}}{T_2} (\frac{\partial T}{\partial z})^2)$  show thermal irreversibility and  $(\frac{\sigma_e B_0^2}{T_2} u^2)$  Joule dissipation irreversibility in Eq. (8),  $p, T, C,$  and  $N$  demonstrated that the pressure, temperature, concentration, and motile microorganisms term,  $\alpha_{\text{trihffd}}$  show that the thermal diffusivity,  $(D_b)_{\text{trihffd}}, (D_n)_{\text{trihffd}}$  represented mass diffusion and motile density of tri hybrid ferrofluid, the thermal conductivity of tri hybrid ferrofluid ( $k_{\text{trihffd}}$ ) are shown by

$$\frac{k_{\text{trihffd}}}{k_{\text{hffd}}} = \frac{k_{s3} + (n_3 - 1)k_{\text{hffd}} - (n_3 - 1)(\phi_3)(k_{\text{hffd}} - k_{s3})}{k_{s3} + (n_3 - 1)k_{\text{hffd}} + (\phi_3)(k_{\text{hffd}} - k_{s3})} \quad (9)$$

$$\frac{k_{\text{hffd}}}{k_{\text{nffd}}} = \frac{k_{s2} + (n_2 - 1)k_{\text{nffd}} - (n_2 - 1)(\phi_2)(k_{\text{nffd}} - k_{s2})}{k_{s2} + (n_2 - 1)k_{\text{nffd}} + (\phi_2)(k_{\text{nffd}} - k_{s2})} \quad (10)$$

$$\frac{k_{\text{nffd}}}{k_{\text{bf}}} = \frac{k_{s1} + (n_1 - 1)k_{\text{bf}} - (n_1 - 1)(\phi_1)(k_{\text{bf}} - k_{s1})}{k_{s1} + (n_1 - 1)k_{\text{bf}} + (\phi_1)(k_{\text{bf}} - k_{s1})} \quad (11)$$

$k_{s1}, k_{s2}, k_{s3}, k_{\text{hffd}}, k_{\text{nffd}}$  and  $k_{\text{bf}}$  are three different types of NPs thermal conductivity of solid, HFFDs, NFFDs, and bases fluid [61]. Furthermore, the ternary hybrid nanolayer thermal conductivity of ferrofluid  $k_{\text{thnffd}}$  are represented by:

$$\frac{k_{\text{trihnlf}}}{k_{\text{hnlf}}} = \frac{(k_{s3} - k_{\text{nlf}})\phi_3 k_{\text{nlf}}((\lambda_2)^2 - (\lambda_1)^2 + 1) + (k_{s3} + k_{\text{nlf}})(\lambda_2)^2(\phi_3(\lambda_1)^2(k_{\text{nlf}} - k_{\text{hnlf}}) + k_{\text{hnlf}})}{(\lambda_2)^2(k_{s3} + k_{\text{nlf}}) - (k_{s3} - k_{\text{nlf}})\phi_3((\lambda_2)^2 - (\lambda_1)^2 - 1)} \quad (12)$$

$$\frac{k_{\text{hnlf}}}{k_{\text{nlf}}} = \frac{(k_{s2} - k_{\text{nlf}})\phi_2 k_{\text{nlf}}((\lambda_2)^2 - (\lambda_1)^2 + 1) + (k_{s2} + k_{\text{nlf}})(\lambda_2)^2(\phi_2(\lambda_1)^2(k_{\text{nlf}} - k_{\text{nlf}}) + k_{\text{nlf}})}{(\lambda_2)^2(k_{s2} + k_{\text{nlf}}) - (k_{s2} - k_{\text{nlf}})\phi_2((\lambda_2)^2 - (\lambda_1)^2 - 1)} \quad (13)$$

$$\frac{k_{\text{nlf}}}{k_{\text{bf}}} = \frac{(k_{s1} - k_{\text{nlf}})\phi_1 k_{\text{nlf}}((\lambda_1)^2 - (\lambda_1)^2 + 1) + (k_{s1} + k_{\text{nlf}})(\lambda_2)^2(\phi_1(\lambda_1)^2(k_{\text{nlf}} - k_{\text{bf}}) + k_{\text{bf}})}{(\lambda_2)^2(k_{s1} + k_{\text{nlf}}) - (k_{s1} - k_{\text{nlf}})\phi_1((\lambda_2)^2 - (\lambda_1)^2 - 1)} \quad (14)$$

Here  $\lambda_1 = 1 + \frac{h}{r}, \lambda_2 = 1 + \frac{h}{2r}$ ,  $h$  shows the nanolayer thickness, and  $r$  represents the radius of the nanoparticle, Figure 2 shows a physical model in a nanolayer with base fluid and nanoparticles  $k_{\text{nlf}} = 3k_{\text{bf}}, k_{\text{hnffd}},$  and  $k_{\text{nffd}}$  are signified by nanolayer, hybrid nanolayer ferrofluid, nanolayer ferrofluid, and base fluid thermal conductivity [62]. Here  $(s'''_{\text{Gen}})_0$  show the initial boundary condition entropy generation:  $(s'''_{\text{Gen}})_0 = \frac{(k_{\text{bf}}(\Delta T)^2)}{s^2 T^2}$ . The flow situation for initial lower and upper boundary conditions is:

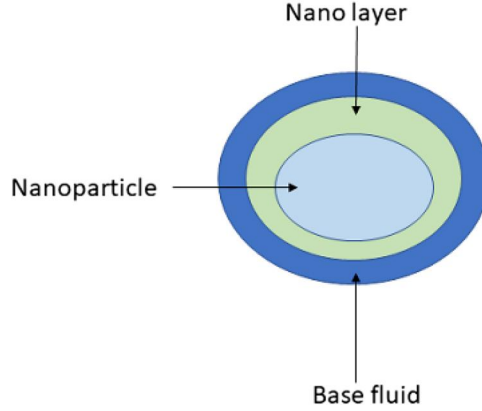


Figure 2. Nanolayer.

$$\begin{aligned} z = -s(t), u = 0, v = -\frac{rA_1s'(t)}{2s}, w = -A_1s'(t), T = T_1, C = C_1, N = N_1, \\ z = s(t), u = 0, v = -\frac{rA_1s'(t)}{2s}, w = A_1s'(t), T = T_2, C = C_2, N = N_2 \end{aligned} \quad (15)$$

The  $s'(t)$  dash here represents the derivative concerning time  $t$ , and  $A_1$  denoted by the permeability measure. Here are the similarity transformation are introduced to get rid of the pressure term:

$$\left. \begin{aligned} \eta = \frac{z}{s}, u = \frac{rv_f}{s^2} F_\eta(\eta, t), v = \frac{rv_f}{s^2} G_\eta(\eta, t), w = \frac{2\nu_f}{s} F(\eta, t), \\ \theta(\eta, t) = \frac{T - T_2}{T_1 - T_2}, \chi(\eta, t) = \frac{C - C_2}{C_1 - C_2}, \psi(\eta, t) = \frac{N - N_2}{N_1 - N_2}. \end{aligned} \right\} \quad (16)$$

Applying this similarity transformation (16) on Eqs. (2–8) then reduce in this form:

$$\frac{\nu_{\text{trihffd}}}{\nu_f} F_{\eta\eta\eta\eta} + \alpha(F_{\eta\eta} + (\eta)F_{\eta\eta\eta}) - 2FF_{\eta\eta\eta} - \frac{s^2}{\nu_f} F_{\eta\eta(t)} + 2GG_\eta - \frac{\rho_f}{\rho_{\text{trihffd}}} MF_{\eta\eta} = 0, \quad (17)$$

$$\frac{\nu_{\text{trihffd}}}{\nu_f} G_{\eta\eta} + \alpha(2G + (\eta)F_\eta) + 2GF_\eta - \frac{s^2}{\nu_f} G_{\eta(t)} - 2FG_\eta - \frac{\rho_f}{\rho_{\text{trihffd}}} MG = 0, \quad (18)$$

$$\theta_{\eta\eta} - \frac{\nu_f}{\alpha_{\text{trihffd}}} (2F - \eta\alpha)\theta_\eta + \left[ (\mu_{\text{trihffd}})(F_{\eta\eta})^2 + M(F_\eta)^2 \right] \frac{k_f}{k_{\text{trihffd}}} (Ec)(Pe) - \frac{a^2}{\rho_{\text{trihffd}}} \theta_t = 0, \quad (19)$$

$$(D_b)_{\text{trihffd}} \chi_{\eta\eta} + \nu_f(\eta\alpha - 2F)\chi_\eta - k^2\chi_t - \frac{a^2}{\nu_f} K_0\chi = 0, \quad (20)$$

$$(D_n)_{\text{trihffd}} \psi_{\eta\eta} + \nu_f(\eta\alpha - 2F)\psi_\eta - k^2\psi_t - bW_c(\psi_\eta\chi_\eta + \psi_{\eta\eta}\chi + N\chi_{\eta\eta}) = 0, \quad (21)$$

$$\begin{aligned} N_s = \frac{s'''_{\text{Gen}}}{(s''_{\text{Gen}})_0} = \frac{k_{\text{trihffd}}}{k_f} (\theta_\eta)^2 + EcPe(\mu_{\text{trihffd}})(\theta + \omega)(F_\eta)^2 \\ + M(S_1)(\theta + \omega)(F_\eta)^2 + \beta_1(\chi_\eta)^2 + \beta_2(\psi_\eta)^2 + \beta_3(\chi_\eta\theta_\eta) + \beta_4(\psi_\eta\theta_\eta), \end{aligned} \quad (22)$$

$$\begin{aligned} \eta = -1, F = -Rey, F_\eta = 0, G = -Rey, \theta = 1, \chi = 1, \psi = 1, \\ \eta = 1, F = Rey, F_\eta = 0, G = Rey, \theta = 0, \chi = 0, \psi = 0. \end{aligned} \quad (23)$$

Here  $\alpha = \frac{ss'(t)}{\nu_f}$  presents wall expansion ratio,  $Rey = \frac{(A_1ss'(t))}{2\nu_f}$  illustrate that the permeable Reynolds number, the parameter for a chemical reaction is shown by  $K_{cr} = K_0 \frac{s^2}{\nu_f(D_n)_{\text{trihffd}}}$ ,

$N = \frac{N_2}{(N_2 - N_1)}$  denote density ratio of microorganisms,  $Pr = \frac{\mu(Cp)_f}{k_f}$  denoted the Prandtl number,  $Ec = \frac{U^2}{(T_1 - T_2)(Cp)_f}$  or  $Sc = \frac{\nu_f}{(D_b)_{\text{trihffid}}}$  represented that the Eckert number and Schmidt number of mass transfer,  $Sn = \frac{n\nu_f}{(D_n)_{\text{trihffid}}}$  represent the Schmidt number density ratio of motile transfer,  $Pe = \frac{bW_c}{(D_n)_{\text{trihffid}}}$  is denoted by Peclet number,  $M = \frac{\sigma_e(B_0)^2 s^2}{\mu_f}$  is the magnetic parameter,  $S_1 = \frac{r^2 \nu_f^2}{k_f s^4}$  show the dimensionless parameter,  $\beta_1 = \frac{RD(C_2 - C_1)T_2^2}{k_f s^2 (\Delta T)^2 C_2}$ ,  $\beta_2 = \frac{RD(N_2 - N_1)T_2^2}{k_f s^2 (\Delta T)^2 N_2}$ ,  $\beta_3 = \frac{RD(C_2 - C_1)T_2}{k_f s^2 (\Delta T)}$ ,  $\beta_4 = \frac{RD(N_2 - N_1)T_2}{k_f s^2 (\Delta T)}$  denoted the motile microorganisms and different nanoparticles diffusivity,  $N_s = \frac{(s''')_{\text{Gen}}}{(s''')_{\text{Gen}}_0}$  show the non-dimensional form of the entropy generation, the entropy generation of upper and lower disk temperature difference is denoted by  $\omega = \frac{T_2}{(T_1 - T_2)}$  and the  $Pe = Rey * Pr$  is the heat transfer of the Peclet number. Consequently, we put  $F = fRey$ ,  $G = gRey$  and use the instance after Majdalani et al. [63] where  $\alpha$  proves to be a constant,  $f = f(\eta)$ ,  $\theta = \theta(\eta)$ ,  $\chi = \chi(\eta)$ ,  $\psi = \psi(\eta)$ , that results in  $\theta_t = 0$ ,  $g_{\eta(t)} = 0$ ,  $f_{\eta(t)} = 0$ ,  $\chi_t = 0$  and  $\psi_t = 0$ . Consequently, we obtain the following equations.

$$\frac{\nu_{\text{trihffid}}}{\nu_f} f'''' + \alpha(3f'' + \eta f''') - 2Rey(ff'' - gg') - \frac{\rho_f}{\rho_{\text{trihffid}}} Mf'' = 0, \quad (24)$$

$$\frac{\nu_{\text{trihffid}}}{\nu_f} g'' + \alpha(2g + \eta f') + 2Rey(gf' - fg') - \frac{\rho_f}{\rho_{\text{trihffid}}} Mg = 0, \quad (25)$$

$$\theta'' + \frac{\nu_f}{\alpha_{\text{trihffid}}} (\eta\alpha - 2Reyf)\theta' + [((\mu_{\text{trihffid}})(f'')^2 + M(f')^2)] \frac{k_f}{k_{\text{trihffid}}} Rey^2 (Ec)(Pe) = 0, \quad (26)$$

$$\chi'' + Sc(\eta\alpha - 2Reyf)\chi' - K_{cr}\chi = 0, \quad (27)$$

$$\psi'' + Sn(\eta\alpha - 2Reyf)\psi' - Pe(\psi'\chi' + \psi''\chi + N\chi'') = 0, \quad (28)$$

$$N_s = \frac{k_{\text{trihffid}}}{k_f} (\theta')^2 + EcPe(\mu_{\text{trihffid}})(\theta + \omega)Rey^2 (f'')^2 + MRey^2 (S_1)(\theta + \omega)(f')^2 + \beta_1(\chi')^2 + \beta_2(\psi')^2 + \beta_3(\chi'\theta') + \beta_4(\psi'\theta'), \quad (29)$$

$$\left. \begin{aligned} \eta = -1, f = -1, f_{\eta} = 0, g = -1, \theta = 1, \chi = 1, \psi = 1, \\ \eta = 1, f = 1, f_{\eta} = 0, g = 1, \theta = 0, \chi = 0, \psi = 0. \end{aligned} \right\} \quad (30)$$

apply the values  $\rho_{\text{trihffid}}$  and  $\nu_{\text{trihffid}}$  of ternary hybrid ferrofluid in Eqs. (24–29) then

$$\frac{(1 + 0.1008((\phi_1)^{0.69574}(dp_1)^{0.44708} + (\phi_2)^{0.69574}(dp_2)^{0.44708} + (\phi_3)^{0.69574}(dp_3)^{0.44708}))}{(\phi_1 \frac{\rho_{s1}}{\rho_{bf}} + \phi_2 \frac{\rho_{s2}}{\rho_{bf}} + \phi_3 \frac{\rho_{s3}}{\rho_{bf}} + (1 - \phi_1 - \phi_2 - \phi_3))} f'''' + \alpha(3f'' + \eta f''') - 2Reyff'' + 2Reygg' - \frac{1}{(\phi_1 \frac{\rho_{s1}}{\rho_{bf}} + \phi_2 \frac{\rho_{s2}}{\rho_{bf}} + \phi_3 \frac{\rho_{s3}}{\rho_{bf}} + (1 - \phi_1 - \phi_2 - \phi_3))} Mf'' = 0 \quad (31)$$

$$\frac{(1 + 0.1008((\phi_1)^{0.69574}(dp_1)^{0.44708} + (\phi_2)^{0.69574}(dp_2)^{0.44708} + (\phi_3)^{0.69574}(dp_3)^{0.44708}))}{(\phi_1 \frac{\rho_{s1}}{\rho_{bf}} + \phi_2 \frac{\rho_{s2}}{\rho_{bf}} + \phi_3 \frac{\rho_{s3}}{\rho_{bf}} + (1 - \phi_1 - \phi_2 - \phi_3))} g'' + \alpha(2g + \eta f') + 2Rey(gf' - fg') - \frac{1}{(\phi_1 \frac{\rho_{s1}}{\rho_{bf}} + \phi_2 \frac{\rho_{s2}}{\rho_{bf}} + \phi_3 \frac{\rho_{s3}}{\rho_{bf}} + (1 - \phi_1 - \phi_2 - \phi_3))} Mg = 0 \quad (32)$$

$$\theta'' + \left( (1 - \phi_1 - \phi_2 - \phi_3) + \phi_1 \frac{(\rho Cp)_{s1}}{(\rho Cp)_{bf}} + \phi_2 \frac{(\rho Cp)_{s2}}{(\rho Cp)_{bf}} + \phi_3 \frac{(\rho Cp)_{s3}}{(\rho Cp)_{bf}} \right) \quad (33)$$

$$Pr(\eta\alpha - 2Reyf) \frac{k_f}{k_{trihffd}} \theta' + [\mu_{trihffd}(f'')^2 + M(f')^2] \frac{k_f}{k_{trihffd}} Rey^2(Ec)(Pe) = 0$$

$$\chi'' + Sc(\eta\alpha - 2Reyf)\chi' - K_{cr}\chi = 0 \quad (34)$$

$$\psi'' + Sn(\eta\alpha - 2Reyf)\psi' - Pe(\psi'\chi' + \psi''\chi + N\chi'') = 0 \quad (35)$$

$$N_s = \frac{k_{trihffd}}{k_f} (\theta')^2 + EcPe\mu_{trihffd}(\theta + \omega)Rey^2(f'')^2 \quad (36)$$

$$+MRey^2(S_1)(\theta + \omega)(f')^2 + \beta_1(\chi')^2 + \beta_2(\psi')^2 + \beta_3(\chi'\theta') + \beta_4(\psi'\theta') \quad (37)$$

$$L_1 = \frac{(1 + 0.1008((\phi_1)^{0.69574}(dp_1)^{0.44708} + (\phi_2)^{0.69574}(dp_2)^{0.44708} + (\phi_3)^{0.69574}(dp_3)^{0.44708}))}{(\phi_1 \frac{\rho_{s1}}{\rho_{bf}} + \phi_2 \frac{\rho_{s2}}{\rho_{bf}} + \phi_3 \frac{\rho_{s3}}{\rho_{bf}} + (1 - \phi_1 - \phi_2 - \phi_3))} \quad (38)$$

$$L_2 = (\phi_1 \frac{\rho_{s1}}{\rho_{bf}} + \phi_2 \frac{\rho_{s2}}{\rho_{bf}} + \phi_3 \frac{\rho_{s3}}{\rho_{bf}} + (1 - \phi_1 - \phi_2 - \phi_3)) \quad (39)$$

$$L_3 = \left( (1 - \phi_1 - \phi_2 - \phi_3) + \phi_1 \frac{(\rho Cp)_{s1}}{(\rho Cp)_{bf}} + \phi_2 \frac{(\rho Cp)_{s2}}{(\rho Cp)_{bf}} + \phi_3 \frac{(\rho Cp)_{s3}}{(\rho Cp)_{bf}} \right) \quad (40)$$

$$L_4 = \frac{k_f}{k_{trihffd}} \quad (41)$$

Putting values of (38), (39), (40), and (41) in Eqs. (31–37) or final result are

$$L_1 f'''' + \alpha(3f'' + \eta f''') - 2Reyff'''' + 2Reygg' - L_2 Mf'' = 0 \quad (42)$$

$$L_1 g'' + \alpha(2g + \eta f') + 2Rey(gf' - fg') - L_2 Mg = 0 \quad (43)$$

$$\theta'' + L_3 L_5 Pr(\eta\alpha - 2Reyf)\theta' + [(\mu_{trihffd})(f'')^2 + M(f')^2] L_5 Rey^2(Ec)(Pe) = 0 \quad (44)$$

$$\chi'' + Sc(\eta\alpha - 2Reyf)\chi' - K_{cr}\chi = 0 \quad (45)$$

$$\psi'' + Sn(\eta\alpha - 2Reyf)\psi' - Pe(\psi'\chi' + \psi''\chi + N_2\chi'') = 0 \quad (46)$$

$$N_s = L_4(\theta')^2 + EcPe(\mu_{trihffd})(\theta + \omega)Rey^2(f'')^2$$

$$+MRey^2(S_1)(\theta + \omega)(f')^2 + \beta_1(\chi')^2 + \beta_2(\psi')^2 + \beta_3(\chi'\theta') + \beta_4(\psi'\theta') \quad (47)$$

### 3. Numerical solution

To obtain a solution using the MATLAB solver `bvp4c`, we can convert Eqs. (42) and (47), which involve 4th and 2nd-order derivatives, into a system of equations with 1st-order derivatives. This conversion allows us to find numerical values for various parameters in tabulation and graphs.

$$f = f(1), f_\eta = f'(1) = f(2), f_{\eta\eta} = f''(2) = f(3), f_{\eta\eta\eta} = f'''(3) = f(4), g = g(5), g_\eta = g'(5) = g(6), \theta = \theta(7),$$

$$\theta_\eta = \theta'(7) = \theta(8), \chi = \chi(9), \chi_\eta = \chi'(9) = \chi(10), \psi = \psi(11), \psi_\eta = \psi'(11) = \psi(12) \quad (48)$$

Now Eqs. (2.42) and (2.46) are changed into 1st order as

$$f'''' = f'(4) = \frac{-\alpha(3f(3) + \eta f(4)) - 2Reyf(1)f(4) + 2Rey g(5)g(6) - L_2 Mf(3)}{L_1} \quad (49)$$

$$g'' = g'(6) = \frac{-\alpha(2g(5) + \eta g(6)) - 2Rey(g(5)f(2) + g(6)f(1)) + L_2Mg(5)}{L_1} \tag{50}$$

$$\theta'' = \theta'(8) = L_3L_5Pr(2Reyf(1) - \alpha\eta)\theta(8) - L_5[L_4f(3)^2 + Mf(2)^2](Rey)^2PrEc \tag{51}$$

$$\chi'' = \chi'(10) = -Sc(\alpha\eta - 2Reyf(1))\chi(10) + K_{cr}\chi(9) \tag{52}$$

$$\psi'' = \psi'(12) = -Sn(\alpha\eta - 2f(1)Rey)\psi(12) + Pe(\psi(12)\chi(10) + \psi'(12)\chi(9) + N_2\chi'(1)) \tag{53}$$

$$N_s = L_4(\theta(8))^2 + EcPe(\mu_{trihffid})(\theta(7) + \omega)Rey^2(f(3))^2 + MRey^2(S_1)(\theta(7) + \omega)(f(2))^2 + \beta_1(\chi(10))^2 + \beta_2(\psi(12))^2 + \beta_3(\chi(10)\theta(8)) + \beta_4(\psi(12)\theta(8)) \tag{54}$$

Boundary conditions for MATLAB are,

$$\eta = -1 = a,$$

$$\eta = 1 = b, fa(1) + 1,$$

$$fa(2), fb(1) - 1, fb(2), fa(5) + 1, fb(5) - 1, fa(7) - 1, fb(7), fa(9) - 1, fb(9), fa(11) - 1, fb(11). \tag{55}$$

We obtained numerical results for shear stress, heat and mass transfer, motile microorganisms, and entropy generation by transforming the equations and boundary conditions into first order. Using MATLAB’s bvp4c solver, we numerically solved the resulting set of dimensionless nonlinear ordinary differential equations and plotted the velocity, temperature, concentration, motility, and entropy generation.

#### 4. Physical parameter

Considering important physical parameter such as skin friction, Nusselt number, Sherwood number, and motile number. These parameters have been approximated for each permeable layer. Both permeable porous disks skin friction are shown  $C_{f(\eta=-1)}, C_{f(\eta=1)}$ , Nusselt number  $Nu_{(\eta=-1)}, Nu_{(\eta=1)}$ , Sherwood number  $Sh_{(\eta=-1)}, Sh_{(\eta=1)}$  and  $Nn_{(\eta=-1)}, Nn_{(\eta=1)}$  of motile number which is expressed as

$$C_{f(\eta=-1)} = \frac{\xi_w}{\rho_{bf}(s'A_1)^2} = \frac{(1 + 0.1008((\phi_1)^{0.69574}(dp_1)^{0.44708} + (\phi_2)^{0.69574}(dp_2)^{0.44708} + (\phi_3)^{0.69574}(dp_3)^{0.44708}))}{Rey_r} \sqrt{f''(-1)^2 + (g'(-1))^2},$$

$$C_{f(\eta=1)} = \frac{\xi_w}{\rho_{bf}(s'A_1)^2} = \frac{(1 + 0.1008((\phi_1)^{0.69574}(dp_1)^{0.44708} + (\phi_2)^{0.69574}(dp_2)^{0.44708} + (\phi_3)^{0.69574}(dp_3)^{0.44708}))}{Rey_r} \sqrt{f''(1)^2 + (g'(1))^2}. \tag{56}$$

The permeable Reynold local number denoted by  $Rey_r = \frac{4s}{r(Re)^2}$ , and shear stress are presented by  $\xi_w$ .  $\xi_w = \sqrt{\xi_{zr}^2 + \xi_{\theta z}^2}$  The direction of radial and tangential represented by  $\xi_{rz}$  and  $\xi_{\theta z}$ , respectively,

$$\begin{aligned}\xi_{rz} &= \mu_{\text{trihffd}} \left( \frac{\partial u}{\partial z} \right) \\ &= \mu_{bf} (1 + 0.1008 ((\phi_1)^{0.69574} (dp_1)^{0.44708} + (\phi_2)^{0.69574} (dp_2)^{0.44708} + (\phi_3)^{0.69574} (dp_3)^{0.44708})) \frac{\nu_f r}{s^3} f''(-1) \\ \xi_{\theta z} &= \mu_{\text{trihffd}} \left( \frac{\partial u}{\partial z} \right) \\ &= \mu_{bf} (1 + 0.1008 ((\phi_1)^{0.69574} (dp_1)^{0.44708} + (\phi_2)^{0.69574} (dp_2)^{0.44708} + (\phi_3)^{0.69574} (dp_3)^{0.44708})) \frac{\nu_f r}{s^3} g'(1)\end{aligned}$$

The Nusselt number top porous disk and bottom porous disk shown by

$$\begin{aligned}Nn_{(\eta=-1)} &= \frac{se_z}{k_f(T_1 - T_2)} = -\frac{k_{\text{trihffd}}}{k_f} \theta'(-1) \\ Nn_{(\eta=1)} &= \frac{se_z}{k_f(T_1 - T_2)} = -\frac{k_{\text{trihffd}}}{k_f} \theta'(1)\end{aligned}\tag{57}$$

Heat flux rate denoted by  $e_z$  for both porous disks.

$$\begin{aligned}e_{z(\eta=-1)} &= -k_{\text{trihffd}} \frac{\partial T}{\partial z} = -k_{\text{trihffd}} \frac{(T_1 - T_2)}{s} \theta'(-1) \\ e_{z(\eta=1)} &= -k_{\text{trihffd}} \frac{\partial T}{\partial z} = -k_{\text{trihffd}} \frac{(T_1 - T_2)}{s} \theta'(1)\end{aligned}$$

The Sherwood number of top and bottom of porous disk mathematical express by

$$\begin{aligned}Sh_{\eta=-1} &= \frac{kq_z}{(D_b)_{\text{trihffd}}(C_1 - C_2)} = -\chi'(-1) \\ Sh_{\eta=1} &= \frac{kq_z}{(D_b)_{\text{trihffd}}(C_1 - C_2)} = -\chi'(1)\end{aligned}\tag{58}$$

where  $q_z$

$$\begin{aligned}q_{z(\eta=-1)} &= -(D_b)_{\text{trihffd}} \frac{\partial C}{\partial z} = -(D_n)_{\text{trihffd}} \frac{(C_1 - C_2)}{k} \chi'(-1) \\ q_{z(\eta=1)} &= -(D_b)_{\text{trihffd}} \frac{\partial C}{\partial z} = -(D_n)_{\text{trihffd}} \frac{(C_1 - C_2)}{k} \chi'(1)\end{aligned}$$

The upward and downward motile number of permeable porous disk are stand by:

$$\begin{aligned}Nn_{(\eta=-1)} &= \frac{kq_n}{(D_n)_{\text{trihffd}}(N_1 - N_2)} = -\psi'(-1) \\ Nn_{(\eta=1)} &= \frac{kq_n}{(D_n)_{\text{trihffd}}(N_1 - N_2)} = -\psi'(1)\end{aligned}\tag{59}$$

where  $q_z$

$$\begin{aligned}q_{z(\eta=-1)} &= -(D_n)_{\text{trihffd}} \frac{\partial N}{\partial z} = -(D_n)_{\text{trihffd}} \frac{(N_1 - N_2)}{k} \psi'(-1) \\ q_{z(\eta=1)} &= -(D_n)_{\text{trihffd}} \frac{\partial N}{\partial z} = -(D_n)_{\text{trihffd}} \frac{(N_1 - N_2)}{k} \psi'(1).\end{aligned}\tag{60}$$

## 5. Result and discussion

This mathematical modeling study presents a boundary value problem for a set of nonlinear ordinary differential equations, which were derived as Eqs. (42–47) to describe the analysis. Due

to the complexity of obtaining an analytical solution, a numerical approach using the BVP4C method is employed. The effects of various physical factors including Peclet number (Pe), magnetic field (M), Eckert number (Ec), Thickness of nanolayer (h), Radius of particles (r), Prandtl number (Pr), Reynolds number (Rey), volume friction  $\phi_1, \phi_2$ , and  $\phi_3$ , density ratio of motile microorganisms (N), shape factor (n), Schmidt number of mass and motile transfer (Sc, Sn), chemical reaction parameter ( $K_{cr}$ ), and expansion ratio parameter ( $\alpha$ ) are displayed in [Figures 3–12](#), showing their impact on different profile. [Tables 2–8](#) offers a concise overview of the numerical consequences stemming from these physical parameters. [Table 2](#) illustrates that when the volume friction, Peclet number, and Eckert number experience escalation, the heat transfer and entropy generation for the upper porous disk also undergo a proportional increase. Physical volume friction refers to the resistance of a fluid to flow, the Peclet number indicates the relative importance of convective to diffusive transport, and the proportion of kinetic energy to enthalpy is represented by the Eckert number. These parameters are crucial in characterizing the behavior of fluids in motion, and they are closely related to the dissipation of energy and the generation of entropy. In the context of ternary hybrid ferrofluids with varying thermal conductivities, an increase in volume friction, Peclet number, and Eckert number leads to higher rates of heat transfer and entropy generation. However, the performance of these fluids is much better when considering thermal nanolayer conductivity, as opposed to overall thermal conductivity. An essential factor that determines the thermal behavior of fluids at the nanoscale is thermal nanolayer conductivity. By improving the thermal nanolayer conductivity of ferrofluids, it is possible to enhance their heat transfer efficiency and reduce the amount of entropy generated during their operation. [Table 3](#) shows that increasing the values of nanolayer thickness reduces the flow of heat transfer rates and enhances the flow of entropy generation in both porous disks. As mentioned earlier, the nanolayer refers to a very thin layer of material with dimensions in the nanometer scale. When the thickness of the nanolayer is increased, the contact area between the materials may be reduced, which can increase the thermal resistance and reduce the heat transfer rate. This can lead to an increase in entropy generation, which is a measure of the disorder or randomness in a system. However, when the values of the radius of particles are increased, the flow of thermal transfer and entropy generation is enhanced in ternary hybrid ferrofluid.

[Table 4](#) demonstrates that the augmentation in the diameter of distinct nanoparticles leads to a reduction in the flow of  $f''(-1)$  and  $g'(-1)$  in both porous disks. The diameter of nanoparticles refers to their size, and it can affect their properties and behavior in a material. However, it amplifies the values of the volume fraction of nanoparticles, increasing the flow of shear and tensional stress. Physically, the volume fraction of distinct nanoparticles refers to the proportion of the total volume of a material that is occupied by the nanoparticles. It is a measure of the concentration or density of nanoparticles in a material. [Table 5](#) represented that the ( $\alpha$ ) varies from  $-ve$  to  $+ve$  values then the flow of fluid has an inverse relationship with  $f''(-1), g'(-1), \theta'(-1), \chi'(-1)$ , and  $\psi'(-1)$  in both upper and lower porous disks, with these parameters decreasing as ( $\alpha$ ) increases. The Reynolds number (Rey) is held constant during this variation of ( $\alpha$ ), and its effect is analyzed by varying Re in further calculations, which indicates the impact of inertia compared to viscosity. By increasing Re, all the aforementioned parameters increase, showing a direct relationship between Re and these parameters. [Table 6](#) presents the effect of the shape factor and volume friction on the Nusselt number (Nu), which is a measure of heat transfer. The volume friction reflects the resistance to flow within the fluid due to its internal frictional forces. As the volume friction grows, the computations' findings demonstrate, the heat transfer efficiency improves in all the shapes considered, including spheres, bricks, cylinders, and platelets. However, the plate-shaped geometry exhibits the highest efficiency among the shapes, as shown by its higher shape factor value ( $n=5.7$ ) in [Table 6](#). This finding means that increasing the volume friction in the plate-shaped geometry leads to the most substantial improvement in heat transfer efficiency compared to the other shapes. Therefore, this information can guide the design

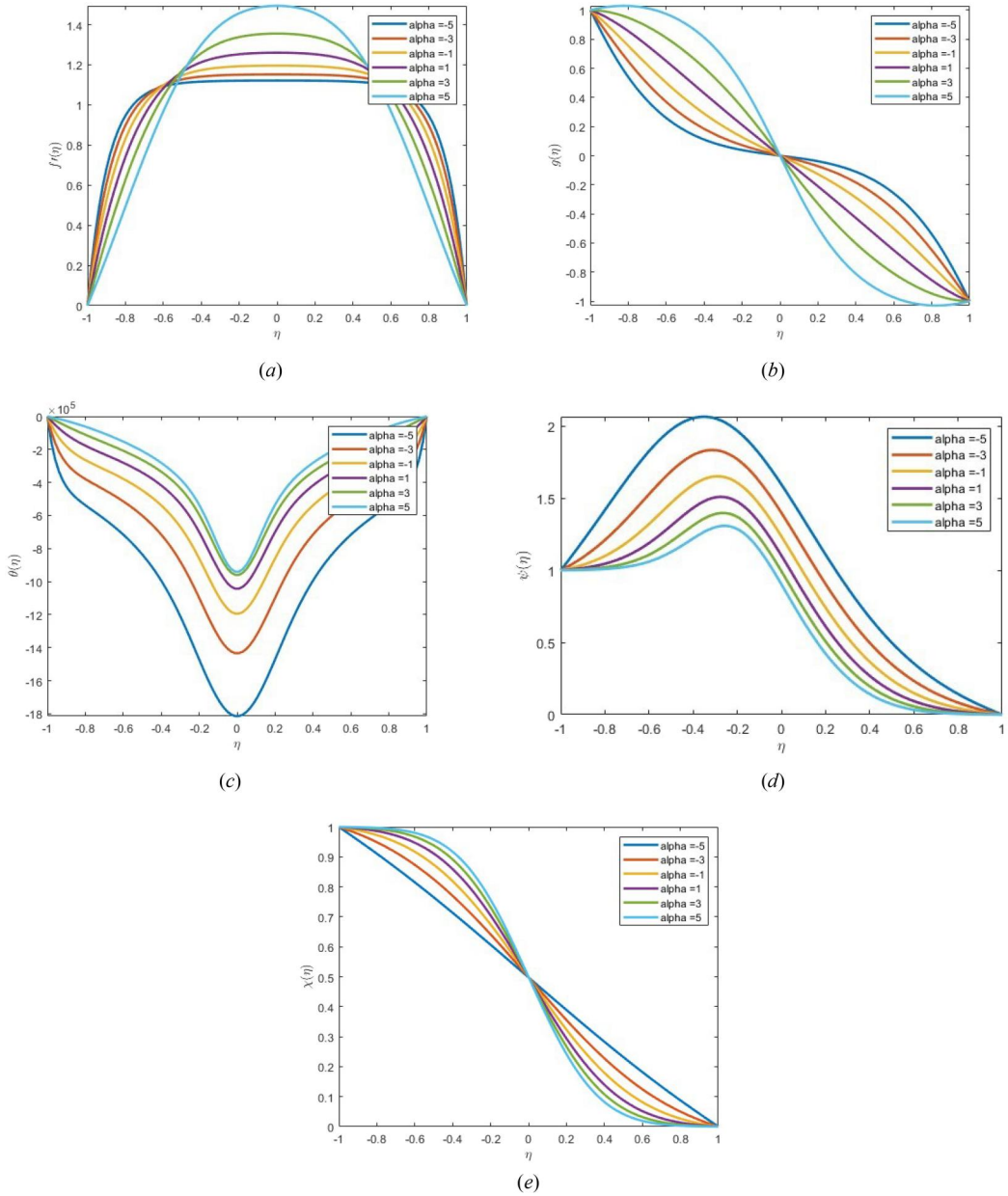


**Figure 3.** Non-dimensional expansion ratio parameter impact in (a) radial velocity profile (b) tangential velocity profile (c) temperature monolayer profile (d) microorganism profile (e) concentration profile for  $\phi_1 = \phi_2 = \phi_3 = 0.02$ ,  $dp_1 = dp_2 = dp_3 = 0.22$ ,  $Rey = 5$ ,  $M = 8$ .

of heat transfer systems to achieve better performance and efficiency in various applications. Table 7 presents the results of calculations carried out to examine the effect of the ( $K_{cr}$ ) on the numerical (She), which characterizes the mass transfer rate. The parameter ( $K_{cr}$ ) represents the chemical reaction rate within the porous disk. The computations were performed while holding the values of other parameters, including  $Rey$ ,  $Sc$ , and  $\alpha$  constant. The findings reveal that an increase in ( $K_{cr}$ ) leads to an increase in  $Sh$  for the lower porous disk. However, for the upper porous disk, the opposite trend is observed, where  $Sh$  decreases with an increase in  $K_{cr}$ .

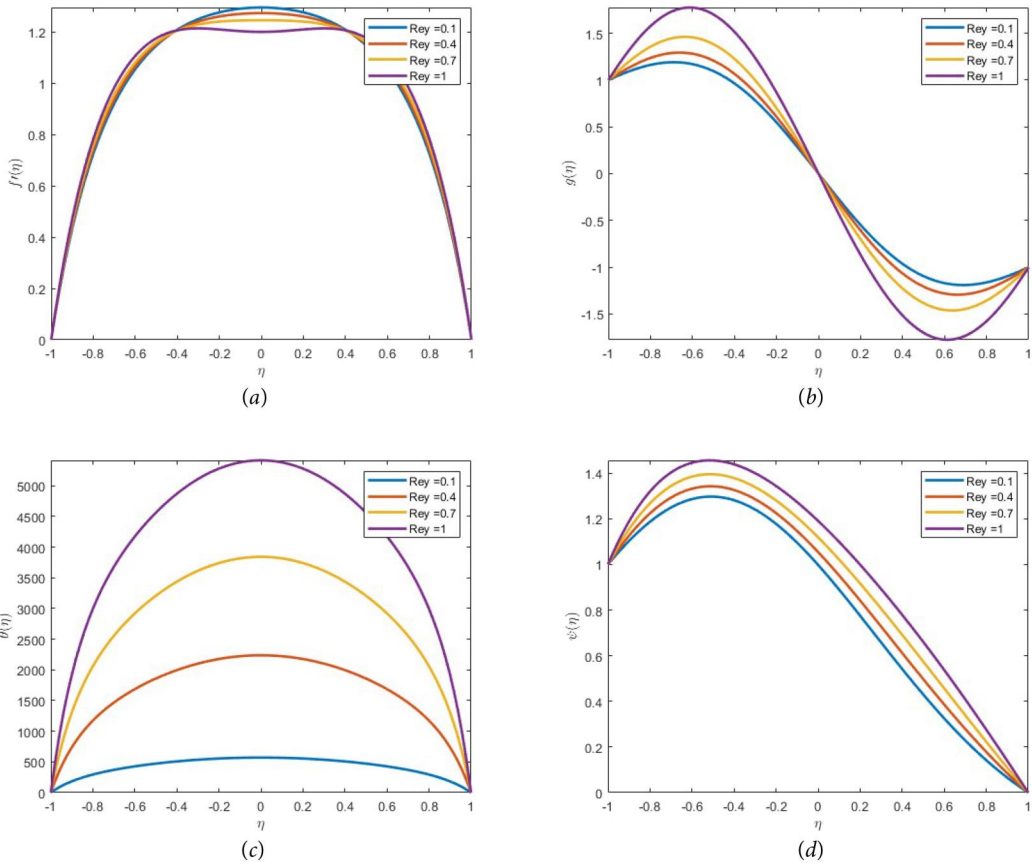


**Figure 4.** Reynolds number parameter impact in (a) radial velocity profile (b) tangential velocity profile (c) temperature profile (d) microorganism profile for  $\phi_1 = \phi_2 = \phi_3 = 0.01, dp_1 = dp_2 = dp_3 = 0.22, \alpha = -2, M = 4$ .

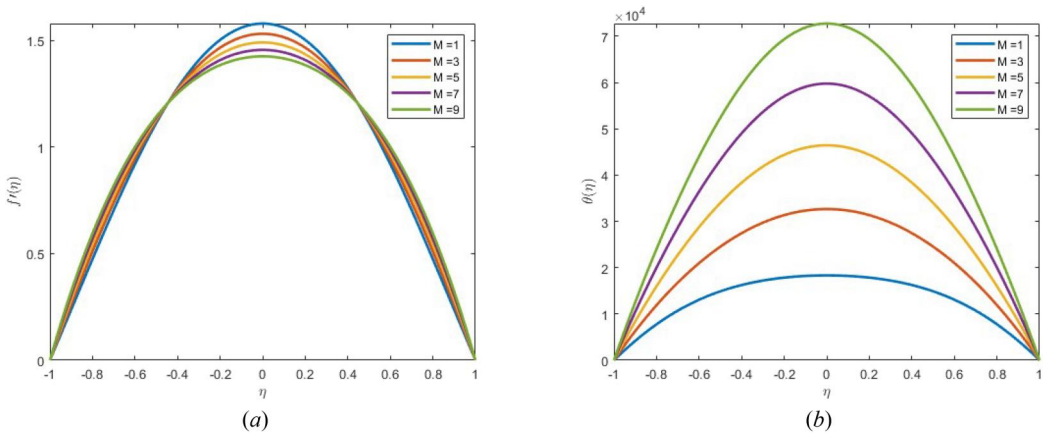


**Figure 5.** Magnetic field parameter impact in (a) radial velocity profile (b) temperature profile for  $\phi_1 = \phi_2 = \phi_3 = 0.01, dp_1 = dp_2 = dp_3 = 0.22, \alpha = -2, Rey = 5$ .

This indicates that the chemical reaction rate within the porous disk influences the mass transfer rate, but the effect varies with the position within the porous disk. Table 8 displays the results of calculations carried out to investigate the impact of varying ( $Sc$ ), ( $Pe$ ), and ( $N$ ) on the motile microorganisms in two different porous disks. The Schmidt number denotes the relationship

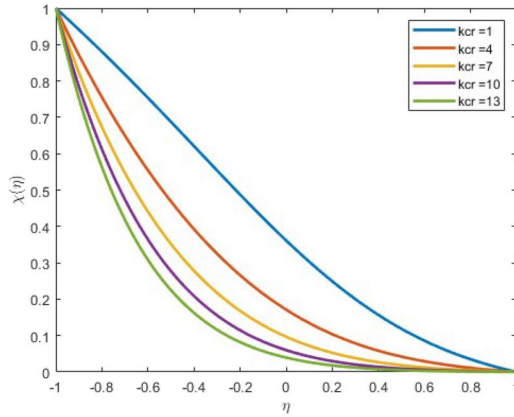


**Figure 6.** Chemical reaction impact in concentration profile for  $\alpha = -1, Re_y = 1, Sc = 1$ .

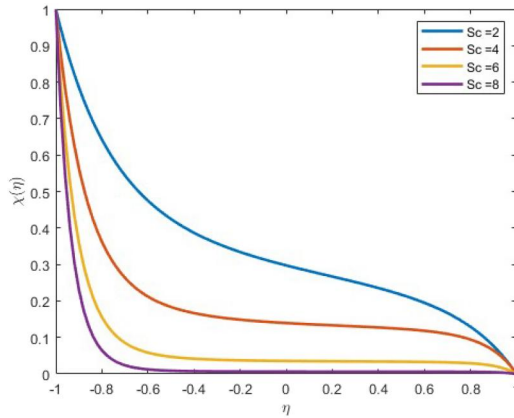


**Figure 7.** Schmidt number of mass transfer impact in concentration profile for  $\alpha = -2, Re_y = 5, K_{er} = 0.1$ .

between momentum diffusivity and mass diffusivity, serving as a dimensionless parameter that delineates the fluid's transport characteristics. The  $Pe$  is a dimensionless parameter that relates the advective and diffusive transport of the fluid. The  $N$  represents the density of the microorganisms relative to that of the surrounding fluid. The outcomes show that as  $Sc$  is raised, while holding the values of  $Pe$  and  $N$  constant, the top and bottom porous disk flow of motile microorganisms decrease, indicating an inverse relationship. Likewise, an escalation in  $Pe$ , while maintaining  $Sc$  and  $(N)$  at a constant level, leads to a reduction in the density of motile microorganisms for the upper permeable disk, and a simultaneous increase for the lower porous disk. Additionally, the calculations were repeated by increasing the value of  $(N)$  while keeping  $Sc$  and  $Pe$  constant. These findings can help optimize the design and operation of various microfluidic systems, such as bioreactors and microfluidic devices for biomedical applications, where precise control over the density of microorganisms is critical. [Table 9](#) demonstrates the validation of the present computed findings by juxtaposing them with the outcomes presented in the study by Ali et al. [57]. The results listed in the table align with each other, confirming their consistency.

The radial velocity in [Figure 3a](#) refers to the velocity component in the radial direction of the fluid flow. Increasing the expansion ratio parameter leads to a reduction in the radial velocity profile. This is because as the flow area increases, the fluid has more space to spread out, which slows down the velocity in the radial direction. The reduction in momentum transfer is a result of the increased drag force exerted on the fluid as it flows through the porous disk, which

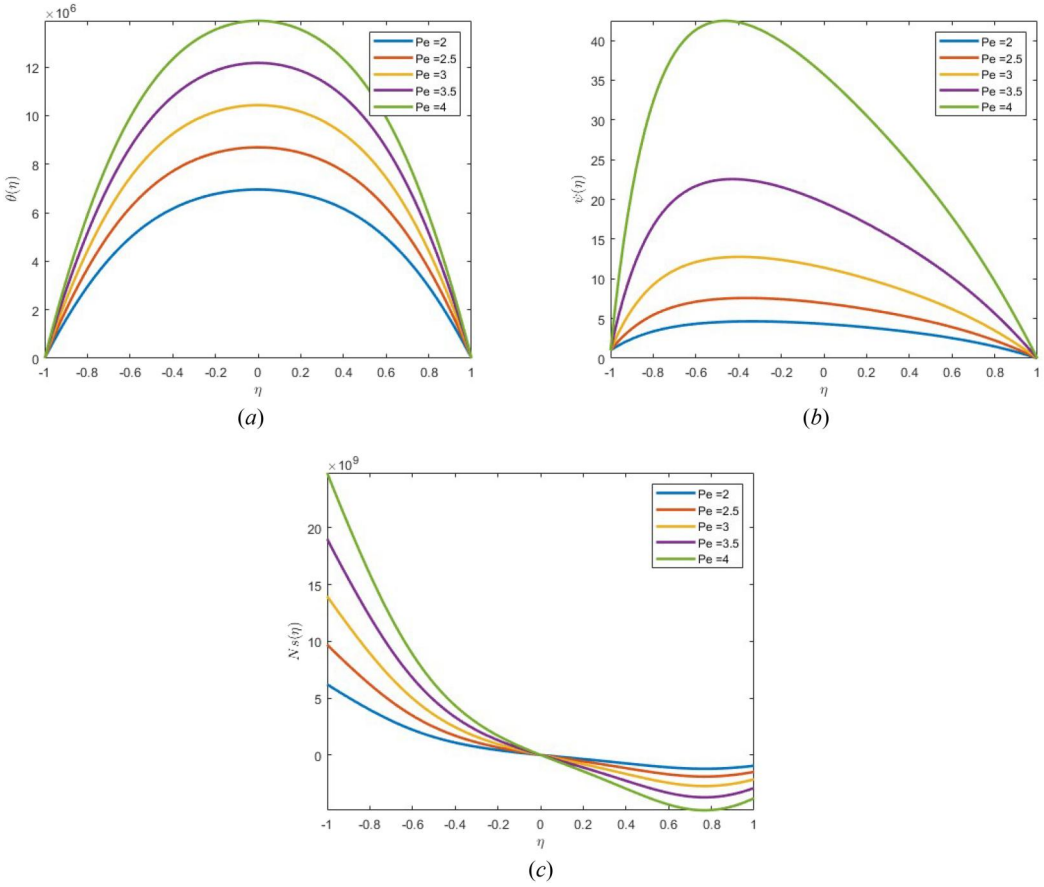


**Figure 8.** Pacllet number effect in (a) temperature profile (b) motile profile (c) entropy generation profile for  $\phi_1 = \phi_2 = \phi_3 = 0.02, h = 1, r = 3, Ec = 8, \alpha = -2, Rey = 2, M = 2$ .

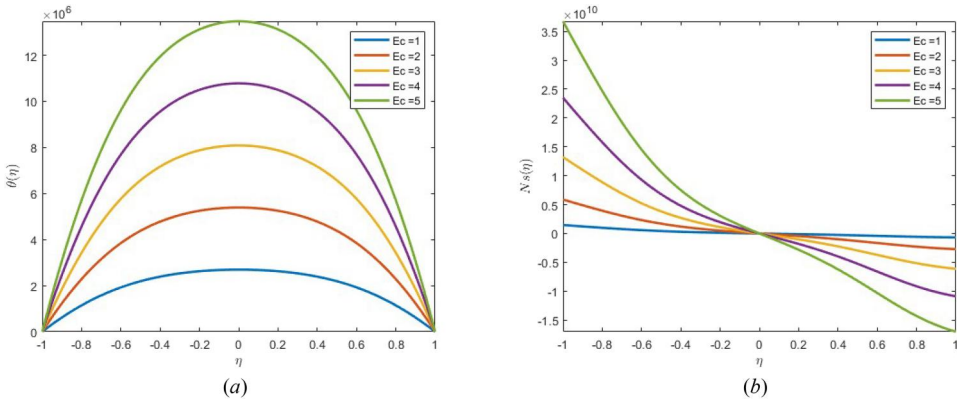


**Figure 9.** Eckert number effect in (a) temperature profile (b) entropy generation profile for  $h = 3, r = 2, \alpha = -3, Rey = 5, M = 2$ .

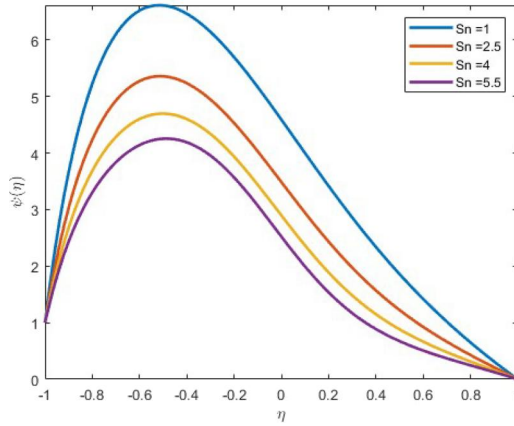


**Figure 10.** Schmidt number of motile transfer effect in microorganism profile for  $Pe = 1, h = 1, r = 2, \alpha = -2, Rey = 2$ .

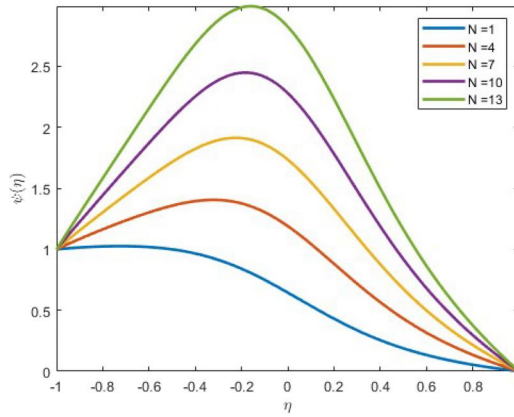


**Figure 11.** Density ratio of motile ( $N$ ) the effect in microorganism profile for  $Pe = 1, h = 5, r = 3, \alpha = -2, Rey = -2$ .

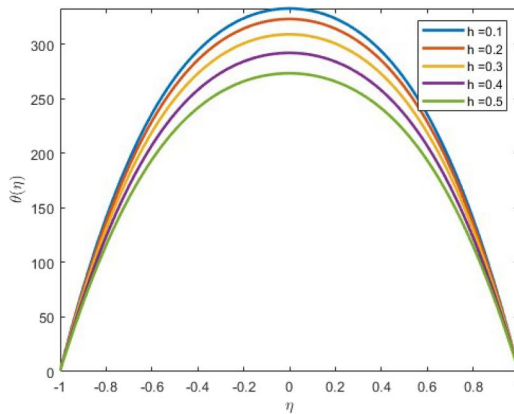


**Figure 12.** Nanolayer effect in temperature profile for  $Pe = 1, r = 3, \alpha = -3, Rey = 5$ .

reduces its velocity. **Figure 3c** shows the impact of the  $\alpha$  parameter on the temperature profile of the fluid. The  $\alpha$  parameter is a measure of the change in the cross-sectional area of the fluid flow passage, and increasing its value reduces the thickness of the thermal boundary layer in both porous disks. The thermal boundary layer is the layer of fluid near the wall where heat is transferred

**Table 2.** Effect of different non-dimensional parameter numerical comparison of ternary hybrid ferrofluid of thermal conductivity (TC) and thermal conductivity of nanolayer (TCN).

$\phi_1 = \phi_2 = \phi_3$	$Pe$	$Ec$	$\theta(1)(TC)$	$N_s(1)(TC)$	$\theta(1)(TCN)$	$N_s(1)(TCN)$
0.01	1	8	10.3905	3.29506	16.8723	3.36937
0.02			10.6344	3.44618	17.4495	3.60397
0.03			10.7737	3.60908	17.6593	3.77996
0.04			11.018	3.73699	18.0265	3.98520
			2	1.49305	0.35449	1.99306
	3	2.65607	1.35541	3.94027	1.4344	
	4	4.16765	3.09216	5.98154	3.3236	
	5	6.37634	5.68884	8.02325	5.96501	
		9	2.2207	4.27695	2.26095	4.45977
		10	2.43506	5.24152	2.50585	5.51756
		11	2.67449	6.37146	2.7595	6.6667
		12	2.87412	7.54781	2.99567	7.97712

**Table 3.** Different non-dimensional parameters  $h$  and  $r$  effect in flow heat transfer and entropy generation for ternary hybrid magnetic fluid.

$h$	$r$	$\theta'(-1)$	$\theta'(1)$	$N_s(-1)$	$N_s(1)$
0.1	0.01	353.097	353.097	-7.72356	-7.72356
0.2		342.773	342.773	-7.53881	-7.53881
0.3		328.319	328.319	-6.80118	-6.80118
0.4		309.753	309.753	-6.24777	-6.24777
	0.03	246.195	246.195	6.4562	6.4562
	0.05	277.693	277.693	7.34409	7.34409
	0.07	289.938	289.938	7.71899	7.71899
	0.09	295.183	295.183	7.95322	7.95322

**Table 4.** Numerical effect of volume friction ( $\phi_1, \phi_2, \phi_3$ ) and diameter of nanoparticles ( $dp_1, dp_2, dp_3$ ) for tri hybrid magnetic fluid flow in lower porous disk shear stress  $f''(-1)$  and tensional stress  $g'(-1)$  for fixed values of  $\alpha = -1, Rey = -1, M = 1$ .

$dp_1 = dp_2 = dp_3$	$\phi_1 = \phi_2 = \phi_3$	$f''(-1)$	$g'(-1)$
0.01	0.01	3.30402	1.65183
0.02		3.30388	1.65159
0.03		3.30377	1.65141
0.04		3.30369	1.65127
		0.02	3.31474
	0.03	3.32496	1.7011
	0.04	3.33471	1.7226
	0.05	3.34398	1.7425

**Table 5.** Calculate the numerical effect of shear stress ( $f''(-1)$ ), tensional stress ( $g'(-1)$ ), heat transfer ( $\theta'(-1)$ ), mass transfer ( $\chi'(-1)$ ), and motile microorganisms ( $\psi'(-1)$ ) different values varies on expansion ratio parameter and permeable Reynolds number for ternary hybrid ferrofluid of the lower porous disk.

$\alpha$	$Rey$	$f''(-1)$	$g'(-1)$	$\theta'(-1)$	$\chi'(-1)$	$\psi'(-1)$	
-2.5	0.01	7.5313	6.0345	233.33	1.8313	9.6652	
-1.5		6.2367	4.5588	16.363	1.4687	7.1742	
-0.5		5.7788	4.2274	7.1141	1.1456	4.8508	
0.5		4.6292	2.9211	2.2368	0.87849	2.9515	
1.5		3.5197	1.5888	1.4392	0.66054	1.5563	
2.5		2.4551	0.2008	0.40872	0.48811	0.65941	
		-2	2.9996	1.3751	0.00496	0.19319	0.15162
		-1.5	3.3147	1.6775	0.03121	0.30748	0.2685
		-1	3.7215	2.0582	0.36469	0.47044	0.58922
		1	4.8562	3.1018	0.58744	0.96884	3.6095
		1.5	5.5919	3.7822	0.89461	1.30514	5.9955
		2	6.5849	4.8547	1.17851	1.4886	7.2512

**Table 6.** Different shape and size factor effect in Nusselt number for tri hybrid ferrofluid ( $\text{Fe}_3\text{O}_4 + \text{CoFe}_2\text{O}_4 + \text{Mn} - \text{ZnFe}_2\text{O}_4 / \text{H}_2\text{O}$ ) thermal nanolayer conductivity.

$\phi_1 = \phi_2 = \phi_3$	$Nu_{(Spherical=3)}$	$Nu_{(Bricks=3.7)}$	$Nu_{(Cylindrical=4.8)}$	$Nu_{(Platelet=5.7)}$
0.01	0.02378	0.02502	0.02698	0.02861
0.02	0.03120	0.03423	0.03917	0.04333
0.03	0.04010	0.04547	0.05429	0.06176
0.04	0.05048	0.05866	0.07206	0.08329
0.05	0.0622	0.05866	0.09198	0.10712

**Table 7.** Sherwood number effect in upper and lower movable porous disks for different values of chemical reaction parameter ( $K_{cr}$ ).

$K_{cr}$	$She_{(\eta=-1)}$	$She_{(\eta=1)}$
2	0.66213	0.06609
4	1.0608	0.03280
6	1.4012	0.01773
8	1.7042	0.01017
10	1.9803	0.00609

**Table 8.** Schmidt number, Peclet number, and density of motile number the effect of microorganisms for both porous disks.

$Sc$	$Pe$	$N$	$Nn_{(\eta=-1)}$	$Nn_{(\eta=1)}$
0.2	0.5	2	0.52419	0.28903
0.4			0.35885	0.2247
0.6			0.22276	0.1675
0.8			0.11305	0.1172
0.2	0.6		0.54596	0.25264
	0.7		0.57345	0.21468
	0.8		0.61073	0.17469
	0.9		0.67007	0.13173
	0.5	2.2	0.51603	0.2848
		2.4	0.50786	0.28058
		2.6	0.49978	0.27635
		2.8	0.49153	0.2721

**Table 9.** Numerical comparison flow of heat and mass for lower porous disk, validity of our work with Ali et al. [57].

$Re$	$f''(-1)$ (Previous work)	Present work	$\theta'(-1)$ (Previous work)	Present work	$\chi'(-1)$ (Previous work)	Present work
-5	3.6501	3.6504	7.6396	7.6399	-0.3960	-0.3958
-3	2.9411	2.9414	3.9055	3.9058	-0.3661	-0.3659
-1	2.3737	2.3740	2.0733	2.0736	-0.3380	-0.3377
0	2.1374	2.1377	1.5333	1.5337	-0.3247	-0.3245
1	1.9289	1.9292	1.1459	1.1462	-0.3118	-0.3115
3	1.5840	1.5844	0.6607	0.6609	-0.2875	-0.2873
5	1.3169	1.3172	0.3975	0.3978	-0.2649	-0.2646

between the fluid and the solid surface. A thinner thermal boundary layer allows for more efficient heat transfer, as there is less resistance to the transfer of thermal energy between the both porous surface. As a result, the temperature profile across the flow passage becomes more uniform, with less variation in temperature between different regions of the flow. Figure 3d illustrates the influence of the  $\alpha$  on the motile microorganism boundary layer thickness and, consequently, the microorganism distribution in a ternary hybrid ferrofluid flowing through two porous disks. Increasing the expansion ratio parameter leads to a reduction in the motile boundary layer thickness and promotes a more uniform distribution of microorganisms across the flow passage. Figure 3e illustrates how the expansion ratio parameter affects the concentration profile of a ternary hybrid ferrofluid in both porous disks. Mass transfer is the movement of particles or substances from one region of the fluid to another, and it is influenced by the concentration

gradient of the fluid. A thinner flow passage reduces mass transfer in the upper disk, leading to a decrease in particle concentration, while the larger flow area in the lower porous disk enhances mass transfer and increases particle concentration. Figures 3b and d show the tensional and concentration profiles of a ternary hybrid ferrofluid, respectively. Increasing the expansion ratio parameter reduces the thickness of the momentum and mass transfer boundary layers in the upper disk, leading to more uniform distribution of fluid velocity and concentration. However, in the lower porous disk, the  $\alpha$  parameter enhances the thickness of both boundary layers, leading to non-uniform distribution of fluid velocity and concentration due to the complex flow behavior in the presence of porous disk. In Figure 4a, c, d, we can see the impact of the Reynolds number on the radial velocity profile, temperature profile, and motile profile. As the Reynolds number increases, the momentum, thermal, and motile boundary layer of the fluid flow increase in both porous disks. This can be explained physically by considering the inertial and viscous forces in the fluid flow. At low Reynolds numbers, the viscous forces dominate, and the fluid flow is laminar and orderly. In this article, we are using Reynolds number  $\geq 2000$  then the fluid flow are laminar. However, as the Reynolds number increases, the inertial forces become more significant, causing the fluid flow to become turbulent and disordered. The increase in momentum boundary layer thickness means that the fluid flow near the surface of the porous disks has more momentum and energy. This results in a higher radial velocity profile, indicating that the fluid is moving faster near the surface of the disks. The increase in thermal boundary layer thickness means that the heat transfer between the fluid and the disks is enhanced. This results in a steeper temperature profile, indicating that there is a greater temperature difference between the fluid and the disks. Finally, the increase in motile boundary layer thickness means that the transport of motile particles in the fluid is improved. This results in a higher motile profile, indicating that there is more mixing and dispersion of the motile particles in the fluid. In summary, the Reynolds number has a significant impact on the radial velocity profile, temperature profile, and motile profile of fluid flow in porous disks. As the Reynolds number increases, the momentum boundary layer, thermal boundary layer, and motile boundary layer thickness increase, leading to faster fluid flow, enhanced heat transfer, and improved mixing of motile particles.

In Figures 5a, b, the magnetic field parameter ( $M$ ) is that it influences the ternary hybrid ferrofluid flow of radial velocity profile and thermal profile in both porous disks. Physically, the magnetic field ( $M$ ) characterizes the influence of magnetic forces on the fluid flow. The chosen range allows for the exploration of both weak and strong magnetic effects, providing insights into the system's response to magnetic fields of varying strengths. As the  $M$  value increases, the momentum and thermal boundary layer thickness of the fluid flow increase, resulting in faster fluid flow near the surface of the disks and enhanced heat transfer between the fluid and the disks. This can be seen in the increase in the radial velocity profile and steeper temperature profile. Therefore, understanding the impact of the magnetic field parameter is essential in studying fluid flow and heat transfer in magnetohydrodynamic systems involving porous disks. Figure 6 illustrates the impact of the chemical reaction parameter ( $K_{cr}$ ) on the concentration profile in porous disks. The figure shows that increasing the value of the chemical reaction parameter reduces the flow of mass transfer in the concentration boundary layer thickness, for both porous disks. Therefore, the physical significance of the chemical reaction parameter is that it plays a crucial role in regulating the mass transfer and concentration profiles in chemical reactions involving porous disks. However, it would typically be chosen based on known reaction kinetics and the expected range of chemical reactivity in the system under investigation. The physical significance of the Schmidt number parameter in Figure 7 is that it represents the ratio of momentum diffusion to mass diffusion in the fluid. As the Schmidt number parameter value increases, the momentum diffusion becomes dominant over mass diffusion, leading to a reduction in the flow of mass transfer in the concentration boundary layer for both porous disks. This results in a decrease in the concentration gradient and concentration profile. Figures 8a–c illustrates the effect

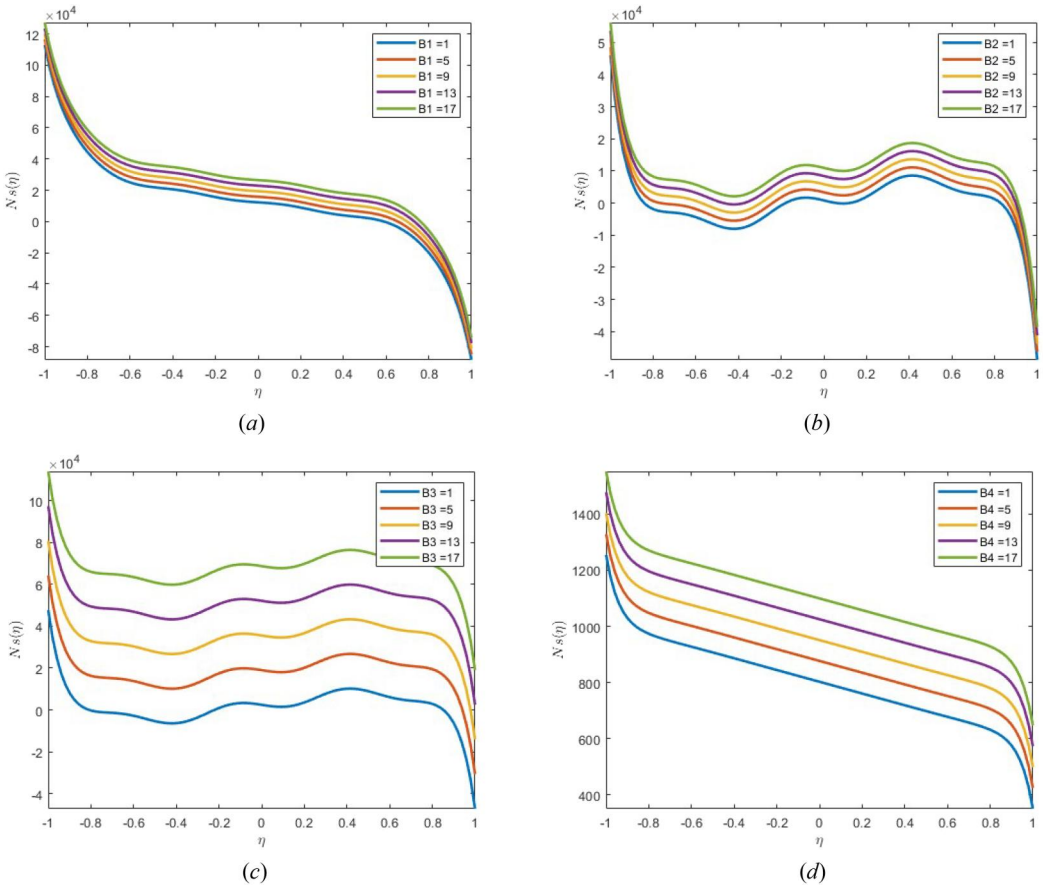


**Figure 13.** Different diffusivity parameters impact in entropy generation profile for  $\phi_1 = \phi_2 = \phi_3 = 0.1, dp_1 = dp_2 = dp_3 = 5, Re_y = 0.2, M = 5$ .

of Peclet number on the temperature profile, motile profile, and entropy generation profile. Physically, the Peclet number is a dimensionless number that represents the ratio of convective transport to diffusive transport. As the Peclet number increases, the flow of thermal and motile transfer increases for both boundary layer thicknesses. This means that the convective heat transfer and fluid motion become more dominant compared to viscous forces. However, the effect on the boundary layer thickness of entropy generation is different for the upper and lower boundaries. As the Peclet number increases, the boundary layer thickness of entropy generation decreases for the upper boundary but increases for the lower boundary.

In [Figures 9a, b](#), the Eckert number is related to its impact on the temperature and entropy generation profiles of the flow. Physically, Eckert number ( $Ec$ ) relates the kinetic energy of fluid motion to the internal energy of the fluid. When the Eckert number is increased, it means that the kinetic energy of the flow is relatively higher compared to its enthalpy. This causes more heat to be transferred across the thermal boundary layer and entropy generation, increasing its boundary layer thickness. Hence, the significance of the Eckert number depicted in [Figures 9a, b](#) is associated with its impact on the equilibrium between kinetic energy and enthalpy within the flow. This, in turn, affects the thickness of both thermal and entropy generation boundary layers, influencing the rates of heat and entropy transfer across these layers. In [Figure 10](#), the physical significance of the Schmidt number is related to its impact on the motion transfer of microorganisms profile in the flow. Physically, the Schmidt number ( $Sc$ ) parameter describes the ratio of

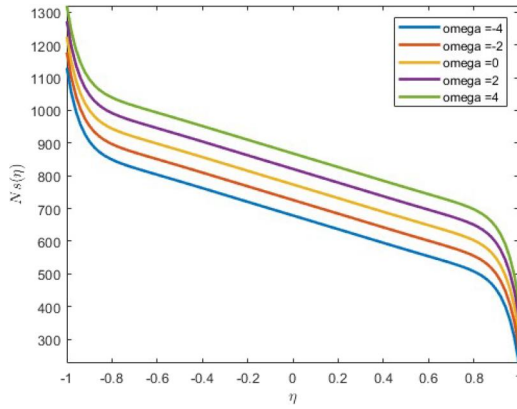


Figure 14. Temperature difference parameters effect in entropy generation profile for  $\phi_1 = \phi_2 = \phi_3 = 0.01, dp_1 = dp_2 = dp_3 = 0.1, Ec = 1, Pe = 1, Rey = 1$ .

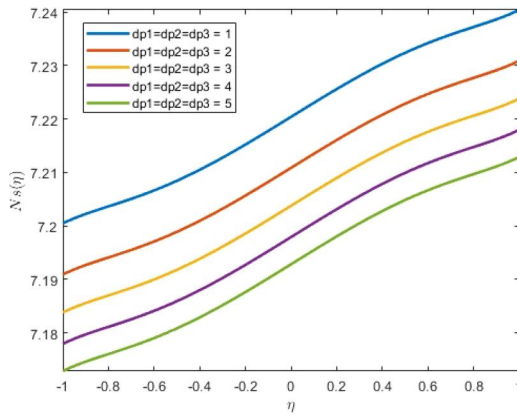


Figure 15. Diameter of different nanoparticles parameters effect in entropy generation profile for  $\phi_1 = \phi_2 = \phi_3 = 0.5, M = 10, Ec = 1, Pe = 1, Rey = 2$ .

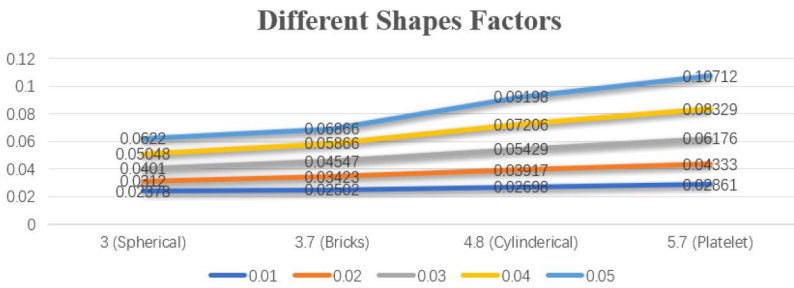


Figure 16. Different shapes and size factor of nanoparticles.

momentum diffusivity to mass diffusivity. When the  $Sc$  is increased, the flow of motile microorganism boundary layer thickness is reduced in both porous disks. This means that a higher Eckert number causes the boundary layer to become thinner, which reduces the transport of microorganisms in the flow. Figure 11 shows that when the motile number density ratio grows, so does the thickness of the microorganism profile boundary layer in both porous disks. This implies that an increase in the number of motile microorganisms in fluid medium results in a thicker boundary layer of microorganisms near a surface, which can impact the transport and diffusion of nutrients and other substances in the surrounding environment.

Figure 12 shows the physical significance of the nanolayer on the temperature profile of the flow. The nanolayer refers to a thin layer of material with a thickness in the nanometer range. When the nanolayer is present, it reduces the thickness of the thermal boundary layer in both porous disks. The thermal boundary layer is the region where heat transfer occurs predominantly by conduction. Faster heat transmission across the both porous surface is the result of the ternary hybrid ferrofluid thermal boundary nanolayer thickness being reduced. Figure 13 illustrates the physical significance of the diffusivity parameter on entropy generation in different parts (a, b, c, d). By enhancing the values of the diffusivity parameters  $\beta_1, \beta_2, \beta_3$ , and  $\beta_4$  we observe an increase in the flow of the fluid, resulting in elevated levels of entropy generation. This implies that higher diffusivity leads to a greater degree of disorder or randomness within the fluid, leading to an increased rate of entropy production. Figure 14 provides a visual representation of the significance of the temperature difference parameter on the entropy generation profile. Furthermore, when the  $\omega$  values exceed zero, it indicates that the flow of the tri-hybrid ferrofluid becomes more pronounced in both porous disks, resulting in an enhanced level of entropy generation. Figure 15 presents the physical interpretation of fluid mechanics in the context of entropy generation. It illustrates that when the parameters associated with different diameter nanoparticles increase, the flow of a viscous fluid is impeded in both porous disks. This decrease in fluid flow leads to a reduction in entropy generation. In fluid mechanics, the size and characteristics of nanoparticles play a role in altering the fluid's behavior and its ability to flow through porous media, ultimately influencing entropy generation in the system. Figure 16 illustrates the use of various shape factors, including spherical, brick-shaped, cylindrical, and platelet shapes. When the volume fraction is increased to 0.05, it is observed that the platelet shape factor results in a higher thermal conductivity flow compared to other shape factors.

## 6. Conclusion

The morphology impact of nanolayer entropy generation on heat and mass transfer, as well as the movement of microorganisms, is examined in a ternary hybrid ferrofluid flow. This research employs a three-dimensional model incorporating Joule heating and viscous dissipation effects in Newtonian fluids. Additionally, it considers chemical reactions taking place within orthogonally moving permeable disks. This study combines the use of several magnetic nanoparticles with flowing water. Several dimensionless parameters are scrutinized to assess their effects on the thickness of the momentum boundary layer, thermal boundary layer, mass transfer boundary layer, microorganism boundary layer, and entropy generation layer. The study shows that the velocity, temperature, concentration, microorganisms, and entropy profiles are significantly affected by the shape of the particles. Following is a summary of the study's findings:

1. Compared to other size factor such as spherical, brick, and cylindrical shapes, the platelets form factor of tri-hybrid ferrofluid ( $\text{Fe}_3\text{O}_4 + \text{CoFe}_2\text{O}_4 + \text{Mn} - \text{ZnFe}_2\text{O}_4/\text{H}_2\text{O}$ ) nanoparticles, with a volume fraction of 5%, demonstrated the highest thermal conductivity within the nanolayer.
2. By increasing the chemical reaction parameter ( $K_{cr}$ ), the value of Sherwood number (Sh) rise proportionally for the both porous disks.
3. Rise the values of different parameter like volume fraction, Peclet number, and Eckert number we analyzed that the flow of heat transfer and entropy generation rate are much better in nanolayer thermal conductivity of ternary hybrid ferrofluid as compared to thermal conductivity.
4. Increasing the diameter of the first, second, and third nanoparticles reduces the flow of shear and tensional stress. However, rising volume fraction values cause an increase in shear and tensional stress flow.

5. Higher values of the Eckert number increase the flow of heat transfer and entropy generation in the boundary layer of both porous disks.
6. Raising the Peclet number improves the flow of temperature profiles and boundary layer thickness in both porous disks, while raising the Schmidt number for mass and motile transfer reduces the flow of concentration and microorganism profiles.
7. Increasing the values of nanolayer particles leads to a reduction in the rate of the temperature profile in both porous disks.
8. If the expansion ratio, Reynold number, and magnetic field number exhibit values greater than zero, then the temperature profile's flow is augmented in both the porous disk with the ternary hybrid ferrofluid.
9. Increasing the values of diffusivity parameters and temperature difference leads to an increase in the flow of entropy generation. However, as the values of different nanoparticle diameters increase, the flow of fluid decreases in both porous disks.

## Disclosure statement

No potential conflict of interest was reported by the author(s).

## Funding

This work is supported by the Fundamental Research Funds for the Central Universities (Grant No. D5000230061).

## ORCID

Qadeer Raza  <http://orcid.org/0009-0008-4831-5606>

Ali J. Chamkha  <http://orcid.org/0000-0002-8335-3121>

## References

- [1] A. Bhandari, "Entropy generation and heat transfer analysis for ferrofluid flow between two rotating disks with variable conductivity," *Proc. Inst. Mech. Eng. C: J. Mech. Eng. Sci.*, vol. 235, no. 21, pp. 5877–5891, 2021. DOI: [10.1177/0954406221991184](https://doi.org/10.1177/0954406221991184).
- [2] N. Acharya, S. Maity and P. K. Kundu, "Entropy generation optimization of unsteady radiative hybrid nanofluid flow over a slippery spinning disk," *Proc. Inst. Mech. Eng. C: J. Mech. Eng. Sci.*, vol. 236, no. 11, pp. 6007–6024, 2022. DOI: [10.1177/09544062211065384](https://doi.org/10.1177/09544062211065384).
- [3] W. Ibrahim and D. Gamachu, "Entropy generation in radiative magneto-hydrodynamic mixed convective flow of viscoelastic hybrid nanofluid over a spinning disk," *Heliyon*, vol. 8, no. 12, pp. e11854, 2022. DOI: [10.1016/j.heliyon.2022.e11854](https://doi.org/10.1016/j.heliyon.2022.e11854).
- [4] M. Ramzan, *et al.*, "Computational Assessment of Carreau Ternary hybrid nanofluid influenced by MHD flow for Entropy generation," *J. Magn. Magn. Mater.*, vol. 567, pp. 170353, 2023. DOI: [10.1016/j.jmmm.2023.170353](https://doi.org/10.1016/j.jmmm.2023.170353).
- [5] R. Agrawal and P. Kaswan, "Entropy generation minimization of  $\text{AgFe}_3\text{O}_4$ /water-ethylene glycol squeezed hybrid nanofluid flow between parallel disks," *HFF*, vol. 33, no. 1, pp. 65–95, 2023. DOI: [10.1108/HFF-01-2022-0005](https://doi.org/10.1108/HFF-01-2022-0005).
- [6] A. Divya and R. B. Reddy, "Electromagnetohydrodynamic unsteady flow with entropy generation and hall current of hybrid nanofluid over a rotating disk: an application in hyperthermia therapeutic aspects," *Proc. Inst. Mech. Eng. C: J. Mech. Eng. Sci.*, vol. 236, no. 13, pp. 7511–7528, 2022. DOI: [10.1177/09544062211076294](https://doi.org/10.1177/09544062211076294).
- [7] G. Ramasekhar and P. B. Reddy, "Entropy generation on EMHD Darcy-Forchheimer flow of Carreau hybrid nanofluid over a permeable rotating disk with radiation and heat generation: homotopy perturbation solution," *Proc. Inst. Mech. Eng. E-J. Pro.*, vol. 237, no. 4, pp. 1179–1191, 2022. DOI: [10.1177/09544089221116575](https://doi.org/10.1177/09544089221116575).

- [8] Z. Shah, A. Shafiq, M. Rooman, M. H. Alshehri and E. Bonyah, "Darcy Forchhemier Prandtl-Eyring nanofluid flow with variable heat transfer and entropy generation using Cattaneo-Christov heat flux model: statistical approach," *Case Stud. Thermal Eng.*, vol. 49, pp. 103376–9, 2023. DOI: [10.1016/j.csite.2023.103376](https://doi.org/10.1016/j.csite.2023.103376).
- [9] U. Farooq, M. I. Afridi, M. Qasim and D. Lu, "Transpiration and viscous dissipation effects on entropy generation in hybrid nanofluid flow over a nonlinear radially stretching disk," *Entropy*, vol. 20, no. 9, pp. 668, 2018. DOI: [10.3390/e20090668](https://doi.org/10.3390/e20090668).
- [10] A. Mahesh, *et al.*, "Significance of non Fourier heat flux and radiation on PEG water based hybrid nanofluid flow among revolving disks with chemical reaction and entropy generation optimization," *Int. Commun. Heat Mass Transf.*, vol. 127, pp. 105572, 2021. DOI: [10.1016/j.icheatmasstransfer.2021.105572](https://doi.org/10.1016/j.icheatmasstransfer.2021.105572).
- [11] M. Arif, *et al.*, "Thermal analysis of viscoelastic radiative flow of tri hybrid nanofluid over a rotating disk using different shaped nanoparticles with applications," *Z. Angew. Math. Mech.*, vol. 103, no. 9, pp. e202200182, 2023. DOI: [10.1002/zamm.202200182](https://doi.org/10.1002/zamm.202200182).
- [12] F. Shahzad *et al.*, "Second-order convergence analysis for Hall effect and electromagnetic force on ternary nanofluid flowing via rotating disk," *Sci. Rep.*, vol.12, no.1, pp. 18769, 2022. DOI: [10.1038/s41598-022-23561-7](https://doi.org/10.1038/s41598-022-23561-7).
- [13] M. D. Shamsuddin, N. Akkurt, A. Saeed and P. Kumam, "Radiation mechanism on dissipative ternary hybrid nanofluid flow through rotating disk encountered by Hall currents: HAM solution," *Alex. Eng. J.*, vol. 65, pp. 543–559, 2023. DOI: [10.1016/j.aej.2022.10.021](https://doi.org/10.1016/j.aej.2022.10.021).
- [14] I. A. Zeeshan, N. Ijaz and A. Majeed, "Analysis of magnetohydrodynamics peristaltic transport of hydrogen bubble in water," *Int. J. Hydrogen Energy*, vol. 43, no. 2, pp. 979–985, 2018. DOI: [10.1016/j.ijhydene.2017.11.095](https://doi.org/10.1016/j.ijhydene.2017.11.095).
- [15] S. Alshahrani, *et al.*, "Numerical simulation of ternary nanofluid flow with multiple slip and thermal jump conditions," *Front. Energy Res.*, vol. 10, pp. 967307, 2022. DOI: [10.3389/feenrg.2022.967307](https://doi.org/10.3389/feenrg.2022.967307).
- [16] M. Usman, M. Areshi, N. Khan and M. S. Eldin, "Revolutionizing heat transfer: exploring ternary hybrid nanofluid slip flow on an inclined rotating disk with thermal radiation and viscous dissipation effects," *J. Thermal Anal. Calorim.*, vol. 148, no. 17, pp. 9131–9144, 2023. DOI: [10.1007/s10973-023-12299-7](https://doi.org/10.1007/s10973-023-12299-7).
- [17] M. M. Alanazi, *et al.*, "Significance of multi hybrid morphology nanoparticles on the dynamics of water fluid subject to thermal and viscous joule performance," *Mathematics*, vol. 10, no. 22, pp. 4259, 2022. DOI: [10.3390/math10224259](https://doi.org/10.3390/math10224259).
- [18] A. Tassaddiq, *et al.*, "Heat and mass transfer together with hybrid nanofluid flow over a rotating disk," *AIP Adv.*, vol. 10, no. 5, pp. 055317, 2020. DOI: [10.1063/5.0010181](https://doi.org/10.1063/5.0010181).
- [19] X. H. Zhang, *et al.*, "The parametric study of hybrid nanofluid flow with heat transition characteristics over a fluctuating spinning disk," *PLoS One*, vol. 16, no. 8, pp. e0254457, 2021. DOI: [10.1002/zamm.202200182](https://doi.org/10.1002/zamm.202200182).
- [20] I. Waini, A. Ishak and I. Pop, "Multiple solutions of the unsteady hybrid nanofluid flow over a rotating disk with stability analysis," *Eur. J. Mech. B/Fluids*, vol. 94, pp. 121–127, 2022. DOI: [10.1016/j.euromechflu.2022.02.011](https://doi.org/10.1016/j.euromechflu.2022.02.011).
- [21] R. Agrawal and P. Kaswan, "Investigation of the heat performance for squeezed hybrid nanofluid flow between parallel disks embedded in porous medium with thermal radiation," *J. Porous Media*, vol. 25, no. 8, pp. 35–53, 2022. DOI: [10.1615/JPorMedia.2022041525](https://doi.org/10.1615/JPorMedia.2022041525).
- [22] A. Zeeshan, M. M. Bhatti, N. Ijaz, O. A. Bég, and A. Kadir, "Biologically inspired transport of solid spherical nanoparticles in an electrically-conducting viscoelastic fluid with heat transfer," *Thermal Sci.*, vol. 24, no. 2 Part B, pp. 1251–1260, 2020. DOI: [10.2298/TSC1180706324Z](https://doi.org/10.2298/TSC1180706324Z).
- [23] K. A. M. Alharbi, N. Ijaz, A. Riaz, F. Altaf and A. Zeeshan, "On multiphase wavy movements of non-Newtonian Jeffery fluid in a rotating channel with MHD and compliant walls: exact solutions," *Waves Random Complex Media*, pp. 1–23, 2022. DOI: [10.1080/17455030.2022.2128230](https://doi.org/10.1080/17455030.2022.2128230).
- [24] A. Majeed, A. Zeeshan and M. Jawad, "Double stratification impact on radiative MHD flow of nanofluid toward a stretchable cylinder under thermophoresis and Brownian motion with multiple slip," *Int. J. Mod. Phys. B*, vol. 37, no. 24, pp. 2350232, 2023. DOI: [10.1142/S0217979223502326](https://doi.org/10.1142/S0217979223502326).
- [25] E. Osalusi, J. Side, R. Harris and B. Johnston, "On the effectiveness of viscous dissipation and Joule heating on steady MHD flow and heat transfer of a Bingham fluid over a porous rotating disk in the presence of Hall and ion-slip currents," *Int. Commun. Heat Mass Transf.*, vol. 34, no. 9–10, pp. 1030–1040, 2007. DOI: [10.1016/j.icheatmasstransfer.2007.05.008](https://doi.org/10.1016/j.icheatmasstransfer.2007.05.008).
- [26] M. F. Iqbal, K. Ali and M. Ashraf, "Heat and mass transfer analysis in unsteady titanium dioxide nanofluid between two orthogonally moving porous coaxial disks: a numerical study," *Can. J. Phys.*, vol. 93, no. 3, pp. 290–299, 2015. DOI: [10.1139/cjp-2014-0243](https://doi.org/10.1139/cjp-2014-0243).
- [27] A. Zeeshan, N. Ijaz, A. Riaz, A. B. Mann and A. Hobiny, "Flow of nonspherical nanoparticles in electromagnetohydrodynamics of nanofluids through a porous medium between eccentric cylinders," *J. Porous Media*, vol. 23, no. 12, pp. 1201–1212, 2020. DOI: [10.1615/JPorMedia.2020024813](https://doi.org/10.1615/JPorMedia.2020024813).
- [28] N. Ijaz, A. Zeeshan, A. Riaz and M. S. Alhodaly, "Transport of drugs using complex peristaltic waves in a biological system," *Waves Random Complex Media*, pp. 1–16, 2022. DOI: [10.1080/17455030.2022.2111031](https://doi.org/10.1080/17455030.2022.2111031).

- [29] M. Shoaib, *et al.*, “Investigation of heat and mass transfer for an MHD hybrid nanofluid flow over a rotating disk: a numerical investigation with supervised neural network,” *Waves Random Complex Media*, vol. 30, pp. 1–24, 2022. DOI: [10.1080/17455030.2022.2128228](https://doi.org/10.1080/17455030.2022.2128228).
- [30] S. Chaudhary and K. K. Chouhan, “Convective heat transfer in magnetohydrodynamic  $TiO_2$ - $CuO$ /ethylene glycol hybrid nanofluid flow toward stagnation point on a radially stretching disk with thermal radiation,” *Heat Transf.*, vol. 51, no. 7, pp. 6320–6339, 2022. DOI: [10.1002/hjt.22593](https://doi.org/10.1002/hjt.22593).
- [31] V. Neha and K. Sharma, “Magnetohydrodynamic hybrid nanofluid flow over a decelerating rotating disk with Soret and Dufour effects,” *MMMS*, vol. 19, no. 2, pp. 253–276, 2023. DOI: [10.1108/MMMS-08-2022-0160](https://doi.org/10.1108/MMMS-08-2022-0160).
- [32] P. S. Reddy, P. Sreedevi and A. J. Chamkha, “MHD boundary layer flow, heat and mass transfer analysis over a rotating disk through porous medium saturated by  $Cu$  –  $water$  and  $Ag$  –  $water$  nanofluid with chemical reaction,” *Powder Technol.*, vol. 307, pp. 46–55, 2017. DOI: [10.1016/j.powtec.2016.11.017](https://doi.org/10.1016/j.powtec.2016.11.017).
- [33] C. Ouyang, *et al.*, “Numerical treatment with Lobatto IIIA technique for radiative flow of MHD hybrid nanofluid ( $Al_2O_3$ - $Cu/H_2O$ ) over a convectively heated stretchable rotating disk with velocity slip effects,” *AIP Adv.*, vol. 10, no. 5, pp. 055122, 2020. DOI: [10.1063/1.5143937](https://doi.org/10.1063/1.5143937).
- [34] R. I. Yahaya, N. M. Arifin, I. Pop, F. M. Ali and S. S. Isa, “Dual solutions for MHD hybrid nanofluid stagnation point flow due to a radially shrinking disk with convective boundary condition,” *HFF*, vol. 33, no. 2, pp. 456–476, 2023. DOI: [10.1108/HFF-05-2022-0301](https://doi.org/10.1108/HFF-05-2022-0301).
- [35] A. Majeed, M. Zubair, A. Khan, T. Muhammad and M. S. Alqarni, “Significance of thermophoretic and Brownian motion on MHD nanofluids flow towards a circular cylinder under the inspiration of multiple slips: an industrial application,” *Math. Probl. Eng.*, vol. 2021, pp. 1–14, 2021. DOI: [10.1155/2021/8634185](https://doi.org/10.1155/2021/8634185).
- [36] M. Z. A. Qureshi, *et al.*, “Morphological nanolayer impact on hybrid nanofluids flow due to dispersion of polymer/CNT matrix nanocomposite material,” *MATH*, vol. 8, no. 1, pp. 633–656, 2023. DOI: [10.3934/math.2023030](https://doi.org/10.3934/math.2023030).
- [37] Q. Raza, *et al.*, “Role of nanolayer on the dynamics of tri-hybrid nanofluid subject to gyrotactic microorganisms and nanoparticles morphology vis two porous disks,” *Case Stud. Thermal Eng.*, vol. 51, pp. 103534, 2023. DOI: [10.1016/j.csite.2023.103534](https://doi.org/10.1016/j.csite.2023.103534).
- [38] N. Acharya, “Spectral simulation to investigate the effects of nanoparticle diameter and nanolayer on the ferrofluid flow over a slippery rotating disk in the presence of low oscillating magnetic field,” *Heat Transf.*, vol. 50, no. 6, pp. 5951–5981, 2021. DOI: [10.1002/hjt.22157](https://doi.org/10.1002/hjt.22157).
- [39] N. Fatima, A. M. Alharbi, N. Ijaz, A. Riaz and E. M. El-Din, “Analysis of rotating-symmetric frame and MHD for peristaltic multiphase flow: an exact solution,” *Front. Phys.*, vol. 11, no. 7, pp. 1, 2023. DOI: [10.3389/fphy.2023.1111163](https://doi.org/10.3389/fphy.2023.1111163).
- [40] N. Ijaz, A. Zeeshan and S. U. Rehman, “Effect of electro-osmosis and mixed convection on nano-bio-fluid with non-spherical particles in a curved channel,” *Mech. Ind.*, vol. 19, no. 1, pp. 108, 2018. DOI: [10.1051/meca/2017040](https://doi.org/10.1051/meca/2017040).
- [41] A. Majeed, S. Rifaqat, A. Zeeshan, M. S. Alhodaly and F. Majeed Noori, “Impact of velocity slip and radiative magnetized Casson nanofluid with chemical reaction towards a nonlinear stretching sheet: three-stage Lobatto collocation scheme,” *Int. J. Mod. Phys. B*, vol. 37, no. 9, pp. 2350088, 4, 2023. DOI: [10.1142/S0217979223500881](https://doi.org/10.1142/S0217979223500881).
- [42] M. Bilal, *et al.*, “Numerical approximation of microorganisms hybrid nanofluid flow induced by a wavy fluctuating spinning disc,” *Coatings*, vol. 11, no. 9, pp. 1032, 2021. DOI: [10.3390/coatings11091032](https://doi.org/10.3390/coatings11091032).
- [43] M. Naveed Khan, S. Ahmad, N. A. Ahammad, T. Alqahtani and S. Algarni, “Numerical investigation of hybrid nanofluid with gyrotactic microorganism and multiple slip conditions through a porous rotating disk,” *Waves Random Complex Media*, vol. 30, pp. 1–16, 2022. DOI: [10.1080/17455030.2022.2055205](https://doi.org/10.1080/17455030.2022.2055205).
- [44] U. Khan, *et al.*, “Dynamics of bio convection agrawal axisymmetric flow of water based  $Cu$ - $TiO_2$  hybrid nanoparticles through a porous moving disk with zero mass flux,” *Chem. Phys.*, vol. 561, pp. 111599, 2022. DOI: [10.1016/j.chemphys.2022.111599](https://doi.org/10.1016/j.chemphys.2022.111599).
- [45] T. Hussain, H. Xu, A. Raees and Q. K. Zhao, “Unsteady three-dimensional MHD flow and heat transfer in porous medium suspended with both microorganisms and nanoparticles due to rotating disks,” *J. Thermal Anal. Calorim.*, vol. 147, no. 2, pp. 1607–1619, 2022. DOI: [10.1007/s10973-020-10528-x](https://doi.org/10.1007/s10973-020-10528-x).
- [46] O. A. Bég, M. N. Kabir, M. J. Uddin, A. Izani Md Ismail and Y. M. Alginahi, “Numerical investigation of Von Karman swirling bioconvective nanofluid transport from a rotating disk in a porous medium with Stefan blowing and anisotropic slip effects,” *Proc. Inst. Mech. Eng. C: J. Mech. Eng. Sci.*, vol. 235, no. 19, pp. 3933–3951, 2021. DOI: [10.1177/0954406220973061](https://doi.org/10.1177/0954406220973061).
- [47] N. Fatima, *et al.*, “Mathematical model for numerical simulations of thermal energy of nano-fluid in a complex peristaltic transport within a curved passage: pharmacological and engineering biomedical application,” *Case Stud. Thermal Eng.*, vol. 45, pp. 102897, 2023. DOI: [10.1016/j.csite.2023.102897](https://doi.org/10.1016/j.csite.2023.102897).

- [48] N. Ijaz, M. M. Bhatti and A. Zeeshan, "Heat transfer analysis in magnetohydrodynamic flow of solid particles in non-Newtonian Ree-Eyring fluid due to peristaltic wave in a channel," *Thermal Sci.*, vol. 23, no. 2 Part B, pp. 1017–1026, 2019. DOI: [10.2298/TSCI1702201551](https://doi.org/10.2298/TSCI1702201551).
- [49] Q. Raza, *et al.*, "Significance role of dual porosity and interfacial nanolayer mechanisms on hybrid nanofluids flow: a symmetry flow model," *Mod. Phys. Lett. B*, vol. 38, no. 8, pp. 2450022, 2023. DOI: [10.1142/S02179849245002222450022-1](https://doi.org/10.1142/S02179849245002222450022-1).
- [50] Y. Li, *et al.*, "Melting thermal transportation in bioconvection Casson nanofluid flow over a nonlinear surface with motile microorganism: application in bioprocessing thermal engineering," *Case Stud. Thermal Eng.*, vol. 49, no. 1, pp. 103285, 2023. DOI: [10.1016/j.csite.2023.103285](https://doi.org/10.1016/j.csite.2023.103285).
- [51] A. Majeed, S. Naeem, A. Zeeshan, A. Qayyum and M. S. Alhodaly, "Three-dimensional bio-convection mechanism and heat transportation of nanofluid induced by magnetic field," *Int. J. Mod. Phys. B*, pp. 2450258, 2023. DOI: [10.1142/S0217979224502588](https://doi.org/10.1142/S0217979224502588).
- [52] N. Fatima, *et al.*, "Three-dimensional analysis of motile-microorganism and heat transportation of viscoelastic nanofluid with nth order chemical reaction subject to variable thermal conductivity," *Case Stud. Thermal Eng.*, vol. 45, no. 1, pp. 102896, 2023. DOI: [10.1016/j.csite.2023.102896](https://doi.org/10.1016/j.csite.2023.102896).
- [53] A. B. Jafar *et al.*, "Mixed convection flow of an electrically conducting viscoelastic fluid past a vertical nonlinearly stretching sheet," *Sci Rep.*, vol. 12, pp. 14679, 2022. DOI: [10.1038/s41598-022-18761-0](https://doi.org/10.1038/s41598-022-18761-0).
- [54] A. Zeeshan, A. Majeed, R. Ellahi and Q. M. Zia, "Mixed convection flow and heat transfer in ferromagnetic fluid over a stretching sheet with partial slip effects," *Thermal Sci.*, vol. 22, no. 6 Part A, pp. 2515–2526, 2018. DOI: [10.2298/TSCI160610268Z](https://doi.org/10.2298/TSCI160610268Z).
- [55] A. Majeed, *et al.*, "Analysis of thermal radiation in magneto-hydrodynamic motile gyrotactic micro-organisms flow comprising tiny nanoparticle towards a nonlinear surface with velocity slip," *Alex. Eng. J.*, vol. 66, no. 1, pp. 543–553, 2023. DOI: [10.1016/j.aej.2022.11.012](https://doi.org/10.1016/j.aej.2022.11.012).
- [56] M. Z. Qureshi, S. Bilal, M. Bilal Ameen, T. Mushtaq and M. Y. Malik, "Numerical examination about entropy generation in magnetically effected hybridized nanofluid flow between orthogonal coaxial porous disks with radiation aspects," *Surf. Interfaces*, vol. 26, pp. 101340, 2021. DOI: [10.1016/j.surfin.2021.101340](https://doi.org/10.1016/j.surfin.2021.101340).
- [57] K. Ali, M. Z. Akbar, M. F. Iqbal and M. Ashraf, "Numerical simulation of heat and mass transfer in unsteady nanofluid between two orthogonally moving porous coaxial disks," *AIP Adv.*, vol. 4, no. 10, pp. 107113, 2014. DOI: [10.1063/1.4897947](https://doi.org/10.1063/1.4897947).
- [58] I. V. Shevchuk, "Modelling of Convective Heat and Mass Transfer in Rotating Flows," Springer International Publishing, pp. 1–235., 2016, DOI: [10.1007/978-3-319-20961-6](https://doi.org/10.1007/978-3-319-20961-6).
- [59] I. V. Shevchuk, "Convective Heat and Mass Transfer in Rotating Disk Systems," Berlin: Springer, vol. 45, 2009, DOI: [10.1007/978-3-642-00718-7](https://doi.org/10.1007/978-3-642-00718-7).
- [60] A. A. Avramenko and I. V. Shevchuk, "Modelling of Convective Heat and Mass Transfer in Nanofluids With and Without Boiling and Condensation," Springer Nature, 2022, DOI: [10.1007/978-3-030-95081-1](https://doi.org/10.1007/978-3-030-95081-1).
- [61] Z. Abdelmalek, M. Z. Qureshi, S. Bilal, Q. Raza and E. S. Sherif, "A case study on morphological aspects of distinct magnetized 3D hybrid nanoparticles on fluid flow between two orthogonal rotating disks: an application of thermal energy systems," *Case Stud. Thermal Eng.*, vol. 23, pp. 100744, 2021. DOI: [10.1016/j.csite.2020.100744](https://doi.org/10.1016/j.csite.2020.100744).
- [62] Q. Raza, *et al.*, "Coaxially swirled porous disks flow simultaneously induced by mixed convection with morphological effect of metallic/metallic oxide nanoparticles," *Front. Mater.*, vol. 10, no. 2, pp. 1152030, 2023. DOI: [10.3389/fmats.2023.1152030](https://doi.org/10.3389/fmats.2023.1152030).
- [63] J. Majdalani, C. Zhou and C. A. Dawson, "The two-dimensional viscous flow between slowly expanding or contracting walls with weak permeability," *J. Biomech.*, vol. 35, no. 10, pp. 1399–1403, 2002. DOI: [10.1016/S0021-9290\(02\)00186-0](https://doi.org/10.1016/S0021-9290(02)00186-0).